ALY688 Protects Against Ferroptosis Via Nrf2 Activation In Skeletal Muscle.

Photsathorn Haetanurak

Thesis submitted to the Faculty of Graduate Studies in Partial Fulfillment of the Requirements for the Degree of Master of Science.

Graduate Program in Biology

York University

Toronto, Ontario

July 2025

Abstract

Ferroptosis is a regulated form of cell death that is characterized by excessive lipid peroxidation. Arachidonic acid (AA), a polyunsaturated fatty acid (PUFA), can be incorporated into cell membrane phospholipids, thereby increasing their susceptibility to oxidative damage and ultimately ferroptosis. In this study, AA was found to enhance susceptibility to ferroptosis in both rat L6 cells and human iPSC-derived skeletal muscle cells. In the presence of AA, cells responded to iron overload (IO) with elevated oxidative stress, total cellular lipid peroxidation and mitochondrial lipid peroxidation, culminating in more ferroptotic cell death. These effects were significantly attenuated by ALY688, an adiponectin receptor agonist. We observed that ALY688 activated Nrf2 signaling in both L6 and iPSC-derived skeletal muscle cells and that the cytoprotective effect of ALY688 was abolished by ML385, an Nrf2 inhibitor. Together, these findings identified that AA increased skeletal muscle cell susceptibility to detrimental effects of iron and established that ALY688 mitigated the combined effects of AA and IO via an Nrf2-dependent mechanism.

Acknowledgements

I would like to express my sincere gratitude to Dr. Gary Sweeney for giving me the opportunity to come to Canada and for his unwavering support throughout the completion of this thesis. His guidance and encouragement have been invaluable to my academic journey. I am also deeply grateful to Dr. Chun Peng for her insightful advice and suggestions, which have greatly helped me achieve my goals. My heartfelt appreciation goes to Dr. Yuqing Feng and Dr. Jennifer L. Kuk for dedicating their time to serve as examiners of my thesis and for their constructive feedback. In my lab, I am especially grateful to Dr. Hyekyoung Sung, who was the very first person to help me become familiar with the lab and who contacted me before I arrived in Canada. Thank you to all current and past members of Sweeney's lab, including Carina Tang, SungJi Cho, Yubin Lei, Trista Chun, Ronke Ayansola, Yue Qu, Michael Sun, and Bojun Zhang, for creating a supportive and collaborative environment. I would like to thank Khang Nguyen for patiently teaching me basic lab skills when I first joined, as I came from a medical background with little laboratory experience. I am also very grateful to Eddie Tam for his help proofreading my thesis and assisting me with various experiments. I would also like to thank Dr. Sivaporn Wannaiampikul for connecting me with Dr. Sweeney, which provided me with the opportunity to study at York University. Finally, I am forever grateful to my parents, Kasem and Sarinee Haetanurak, for their financial and emotional support throughout this journey. I would also like to thank my girlfriend, Wuttidaporn Siriwut, whose unwavering support helped me adapt and persevere during my two years in this country. Without your encouragement, I would not have been able to stay and succeed here.

Table of Contents

List of Figures

List of tables

Chapter 1: Literature review

1.1 Metabolic syndrome and Metabolic Hyperferritinemia

Metabolic syndrome (MetS) is a cluster of metabolic abnormalities that increase the risk of cardiovascular disease, type 2 diabetes, and their related complications. While definitions may vary slightly among organizations, the core components consistently include abdominal obesity, dyslipidemia, hypertension, and impaired glucose metabolism. [1-4]. The National Cholesterol Education Program Adult Treatment Panel III (NCEP ATP III) defines metabolic syndrome as the presence of at least three out of five criteria: (1) abdominal obesity, defined as a waist circumference >102 cm (40 in) in men or >88 cm (35 in) in women; (2) elevated triglycerides (≥150 mg/dL); (3) reduced HDL cholesterol (<40 mg/dL in men or <50 mg/dL in women); (4) hypertension (blood pressure ≥130/85 mmHg); and (5) elevated fasting glucose (≥100 mg/dL) or the use of glucose-lowering therapy (Figure 1) [1, 5]. Later, the American Heart Association/National Heart, Lung, and Blood Institute (AHA/NHLBI) updated the ATP III criteria by lowering the fasting glucose threshold to 100 mg/dL, allowing ethnic-specific waist circumference adjustments (e.g., ≥90 cm for Asian men), and recognizing medication-treated lipid and blood pressure abnormalities as qualifying factors for diagnosis. [3]. Furthermore, the International Diabetes Federation (IDF) introduced a definition particularly relevant to European populations, which requires central obesity as a mandatory criterion, defined by waist circumference thresholds of ≥94 cm for men and ≥80 cm for women, along with at least two additional components from elevated triglycerides, low HDL cholesterol, elevated blood pressure, or elevated fasting glucose

[4]. This differs from U.S.-based definitions (e.g., NCEP ATP III and AHA/NHLBI), which do not require central obesity as a prerequisite for diagnosis. The prevalence of metabolic syndrome among Canadian adults varies depending on the diagnostic criteria. According to the NCEP ATP III definition, the estimated prevalence is approximately 14.9%, whereas the IDF criteria yield a higher estimate of 22.3% [6, 7]. Although the prevalence in Canada is lower than that in the United States, where estimates range from 32.3% to 34.4% [7], the health impact remains substantial. The increased risks associated with metabolic syndrome have significant clinical implications, as chronic diseases related to MetS account for 43% of all deaths in Canada and contribute to 17% of the total healthcare costs [6]. Cardiovascular disease and type 2 diabetes are among the most well-established complications of metabolic syndrome; however, iron overload has recently emerged as an important and newly recognized complication.

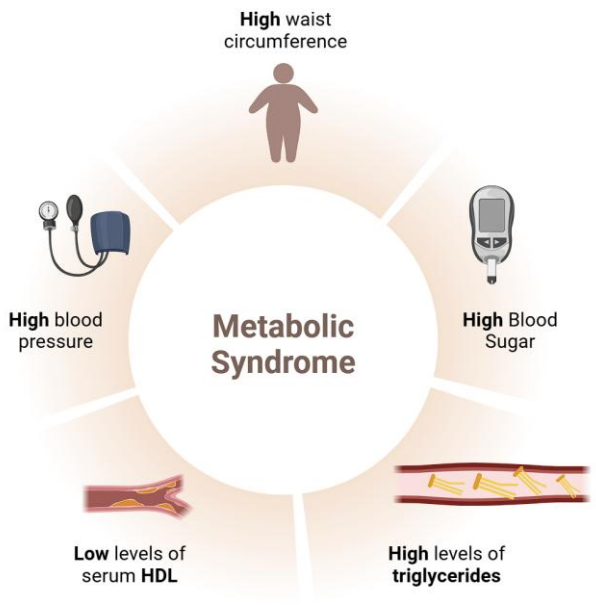

Figure 1: **Diagnostic criteria of metabolic syndrome based on *The National Cholesterol Education Program Adult Treatment Panel III (NCEP ATP III)***

This diagram illustrates the NCEP ATP III diagnostic criteria for the metabolic syndrome. According to this classification, a diagnosis of metabolic syndrome is made when at least three out of the following five criteria are present: (1) abdominal obesity, defined as a waist circumference >102 cm (40 in) in men or >88 cm (35 in) in women; (2) elevated triglycerides (≥150 mg/dL); (3) reduced HDL cholesterol (<40 mg/dL in men or <50 mg/dL in women); (4) hypertension (blood pressure ≥130/85 mmHg); and (5) elevated fasting glucose (≥100 mg/dL) or the use of glucose-lowering therapy

Ferritin, the primary iron storage protein, is a key biomarker for assessing iron levels in the body. Studies have identified hyperferritinemia, elevated ferritin levels, in chronic inflammatory conditions such as type 2 diabetes, obesity, and fatty liver disease [8-11]. The relationship between metabolic dysfunction and iron accumulation in metabolic syndrome appears to be bidirectional: excess iron can contribute to insulin resistance through oxidative stress mechanisms, whereas metabolic dysfunction can

promote iron accumulation [12, 13]. Mendler and colleagues first noticed a link between liver iron overload and insulin resistance. They observed that patients with mild-to-moderate iron overload often had insulin resistance. This condition is known as insulin resistance-associated hepatic iron overload [14, 15]. As our understanding of this condition has grown, its terminology has evolved to reflect its broader metabolic context. It was widely recognized as dysmetabolic iron overload syndrome (DIOS), which includes insulin resistance and other metabolic abnormalities, such as obesity, dyslipidemia, hypertension, and fatty liver disease [16]. However, DIOS primarily focuses on histologically confirmed hepatic iron overload, often requiring invasive procedures such as liver biopsy. This limitation reduces its effectiveness in the early detection of diseases and may result in the oversight of patients with subclinical or early stage disease [13, 17]. In 2023, a multidisciplinary global panel of experts introduced the term metabolic hyperferritinemia (MHF) in a consensus statement aimed at improving diagnosis and clinical management of this condition. The proposed diagnostic criteria for MHF include hyperferritinemia, defined as serum ferritin >300 ng/mL in men and >200 ng/mL in women, along with evidence of fatty liver, type 2 diabetes, obesity, or at least two other features of metabolic dysfunction associated with insulin resistance. Importantly, patients must not have any history of or current hematological diseases [13]. MHF can be further classified into three stages, as outlined in Table 1, to guide disease monitoring and management.

Stage	Ferritin (ng/mL)	Hepatic Iron (MRI R2* s^{-1})	Organ damage related to iron
1. MHF	200–550 (F), 300–550 (M)	<70	Usually absent
2. Dysmetabolic iron accumulation	550–1000	70–140	Rare
3. DIOS	>1000	>140	Present

Table 1: Staging of metabolic hyperferritinemia (MHF)

This table illustrates the staging of metabolic hyperferritinemia (MHF) based on the plasma ferritin levels. It also includes the corresponding measurements of hepatic iron content assessed using magnetic resonance imaging (MRI). Additionally, the graph highlights the progression to organ damage, which may involve the liver, pancreas, heart, and other tissues commonly affected by iron overload and metabolic dysfunction.

The pathophysiology of metabolic hyperferritinaemia (MHF) has been found to be closely associated with hepcidin resistance [13]. This mechanism distinguishes MHF from hematological conditions such as hereditary hemochromatosis, despite both being linked to iron overload in the context of the metabolic syndrome [18, 19]. Hepcidin, a 25-amino acid peptide hormone, plays a central role in regulating systemic iron metabolism in humans. It maintains iron homeostasis by controlling absorption, recycling, and storage, thereby preventing iron deficiency and toxicity [20]. In MHF, hepcidin resistance arises from metabolic stressors such as hyperinsulinemia and lipotoxicity, which impair the hepcidin–ferroportin signaling pathway. This disruption affects intestinal iron absorption and iron release from hepatic macrophages (Kupffer cells), leading to dysregulated iron accumulation [13, 21] (Figure 2).

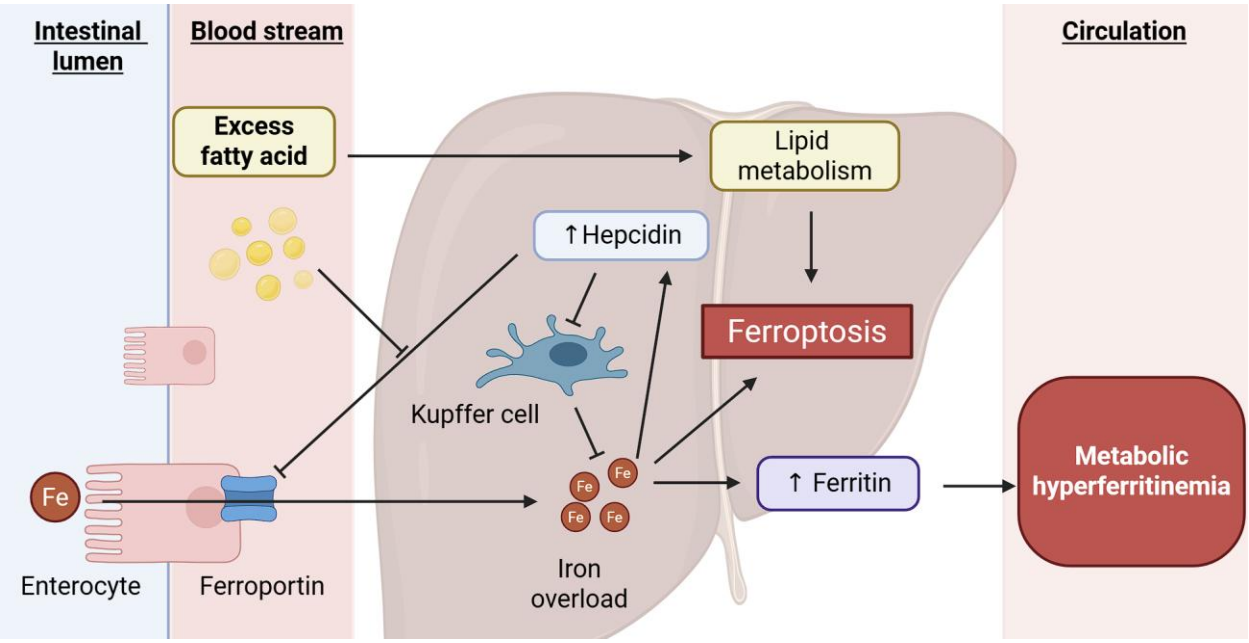

Figure 2: Pathophysiology of metabolic hyperferritinemia

This diagram illustrates how alterations in hepatic lipid metabolism, when combined with excessive iron and lipid intake, lead to iron accumulation in various tissues, including liver. This accumulation exacerbates insulin resistance and may contribute to the progression of type 2 diabetes. Image adapted from Valenti, L., et al (2023) [13]

The diagram also suggests that excess iron can circulate in the bloodstream and affect other organs, such as the skeletal muscle. In skeletal muscle, elevated iron levels disrupt glucose homeostasis and impair metabolic function, contributing to a decline in muscle performance and overall function [22-24]. Animal studies, particularly in mice, have demonstrated that iron overload can lead to muscle atrophy and a progressive loss of muscle mass [25]. This loss of muscle mass and strength is known as sarcopenia [24, 26]. Several studies have reported that individuals with both sarcopenia and metabolic syndrome frequently exhibit iron overload [23, 24, 26], suggesting a

potential association. These findings imply that conditions such as metabolic hyperferritinemia (MHF) and dysmetabolic iron overload syndrome (DIOS) may contribute to the development or progression of sarcopenia.

1.2 Ferroptosis and skeletal muscle

Iron is an indispensable element in human biology and participates in essential processes such as oxygen transport, DNA synthesis, and cellular respiration [27, 28]. Its unique redox properties allow it to function as both an electron carrier and cofactor in numerous enzymatic reactions. To maintain cellular homeostasis, iron is tightly regulated through specialized storage and transport systems [29]. Disruption of iron homeostasis can lead to various pathological conditions. The classical disorder associated with iron overload is hereditary hemochromatosis, resulting from mutations in genes that regulate hepcidin production or its interaction with ferroportin. These mutations lead to inappropriate intestinal iron absorption and systemic iron accumulation [30, 31]. Excess iron is then deposited in multiple organs, potentially resulting in cirrhosis, diabetes, arthritis, and cardiomyopathy [32]. As discussed in the previous section, MHF represents another example of an iron overload-related disease, although it arises from a different pathophysiological mechanism [33, 34].

Ferroptosis is a distinct form of regulated cell death characterized by iron and the accumulation of lipid peroxidation. This mechanism was first identified in 2012 by Dr. Scott J. Dixon and colleagues demonstrated that ferroptosis is mechanistically distinct from other forms of programmed cell death [25, 35, 36]. Dixon's team showed that

ferroptosis is marked by reduced activity of glutathione peroxidase 4 (GPX4) and the accumulation of oxidized Fe^{2+}, which catalyzes the formation of reactive oxygen species (ROS) via the Fenton reaction [36, 37]. These features distinguish ferroptosis from apoptosis, necrosis, and autophagy processes. There are three primary mechanisms contribute to ferroptosis [35, 36, 38, 39]. The first involves lipid peroxidation, primarily driven by the metabolism of polyunsaturated fatty acids (PUFAs) [40]. Under normal conditions, PUFAs contribute to the structural integrity of the cell membrane, particularly the phospholipid bilayer. However, excessive lipid intake or metabolic imbalance can lead to uncontrolled lipid peroxidation [41]. Among PUFAs, arachidonic acid (AA) is the major substrate for lipid peroxidation. AA is esterified into phosphatidylethanolamine (PE), which forms AA-PE, a key effector of cell membrane oxidative degradation [42, 43]. When PUFAs are absorbed into the cell, they are first activated through esterification into PUFA-CoA by ACSL4 (acyl-CoA synthetase long-chain family member 4). ACSL4 preferentially activates long-chain PUFAs, such as AA and adrenic acid (AdA), generating PUFA-CoA substrates that sensitize the membranes to ferroptotic damage. Subsequently, LPCAT3 (lysophosphatidylcholine acyltransferase 3) incorporates these activated PUFAs into phospholipids by converting lysophosphatidylethanolamine (lyso-PE) into PUFA-PE. These PUFA-containing phospholipids are highly susceptible to peroxidation, either enzymatically via lipoxygenases or non-enzymatically via iron-mediated Fenton reactions. Together, ACSL4 and LPCAT3 drive the lipid remodeling process that enriches membranes with oxidizable PUFA-PE species, thereby playing a central role in lipid peroxidation and determining cellular sensitivity to ferroptosis [24, 25, 38]. (Figure 3)

Abnormal iron homeostasis is a key mechanism contributing to ferroptosis. Iron homeostasis is maintained through four interconnected processes: uptake, storage, utilization, and efflux. Most cells acquire iron via two primary pathways: transferrin (TF)-bound iron uptake and non-TF-bound iron (NTBI) uptake [44]. Under iron overload conditions, transferrin becomes saturated, leading to an increase in NTBI. This excess NTBI enters cells through transmembrane iron transporters, such as SLC11A2 (also known as DMT1) [45]. Once inside the cell, iron is primarily stored in ferritin and the labile iron pool (LIP) [46]. Approximately 70–80% of intracellular iron is stored in ferritin [42], which plays a critical role in preventing the oxidative damage. Ferritin is composed of two subunits: ferritin heavy chain 1 (FTH1) and ferritin light chain (FTL) [47]. FTH1 catalyzes the oxidation of Fe^{2+} to Fe^{3+}, whereas FTL contributes to iron nucleation and mineralization. These subunits assemble into a spherical shell capable of storing up to 4,000 iron atoms [36, 39]. Ferritin is essential for minimizing iron-induced oxidative stress. The downregulation of ferritin impairs this protective capacity, rendering cells more vulnerable to oxidative damage and ferroptosis [48, 49]. LIP, consisting of readily available Fe^{2+}, can be stored, exported, or utilized to meet metabolic needs [42]. Within the LIP, ferrous iron binds to iron chaperones, such as poly(rC)-binding proteins (PCBPs). Specifically, PCBP1 and PCBP2 regulate the metalation of iron-dependent enzymes and direct the trafficking of Fe^{2+} for storage or export [44, 50]. Notably, PCBP1 has been shown to inhibit ferroptotic cell death in several studies [51, 52]. Iron from the LIP is primarily directed to the mitochondria, where it supports vital enzymatic functions, including redox reactions, energy metabolism, and DNA synthesis [53]. However, when iron accumulates excessively or ferritin is degraded, the resulting increase in free labile

iron promotes reactive oxygen species (ROS) generation via the Fenton reaction, which significantly contributes to ferroptosis [42, 54, 55]. (Figure 3)

The final key mechanism of ferroptosis is related to the antioxidant defense system. Glutathione peroxidase 4 (GPX4) is a critical enzyme that inhibits the formation of lipid peroxides, thereby protecting cells from ferroptotic damage. GPX4 functions by converting glutathione (GSH) into oxidized glutathione (GSSG) while simultaneously reducing cytotoxic lipid hydroperoxides (L-OOH) to their corresponding non-toxic alcohols (L-OH) [24, 35, 56]. Glutathione synthesis depends on the availability of cystine, which is imported into the cell via System Xc^-, an antiporter that exchanges extracellular cystine for intracellular glutamate [45]. Inhibition of the System Xc^- antiporter leads to glutathione depletion, impaired GPX4 activity, and ultimately ferroptotic cell death. This mechanism is of particular interest in cancer therapy, as some anti-cancer drugs are designed to inhibit System Xc^- and thereby induce ferroptosis selectively in tumor cells [46] (Figure 3)

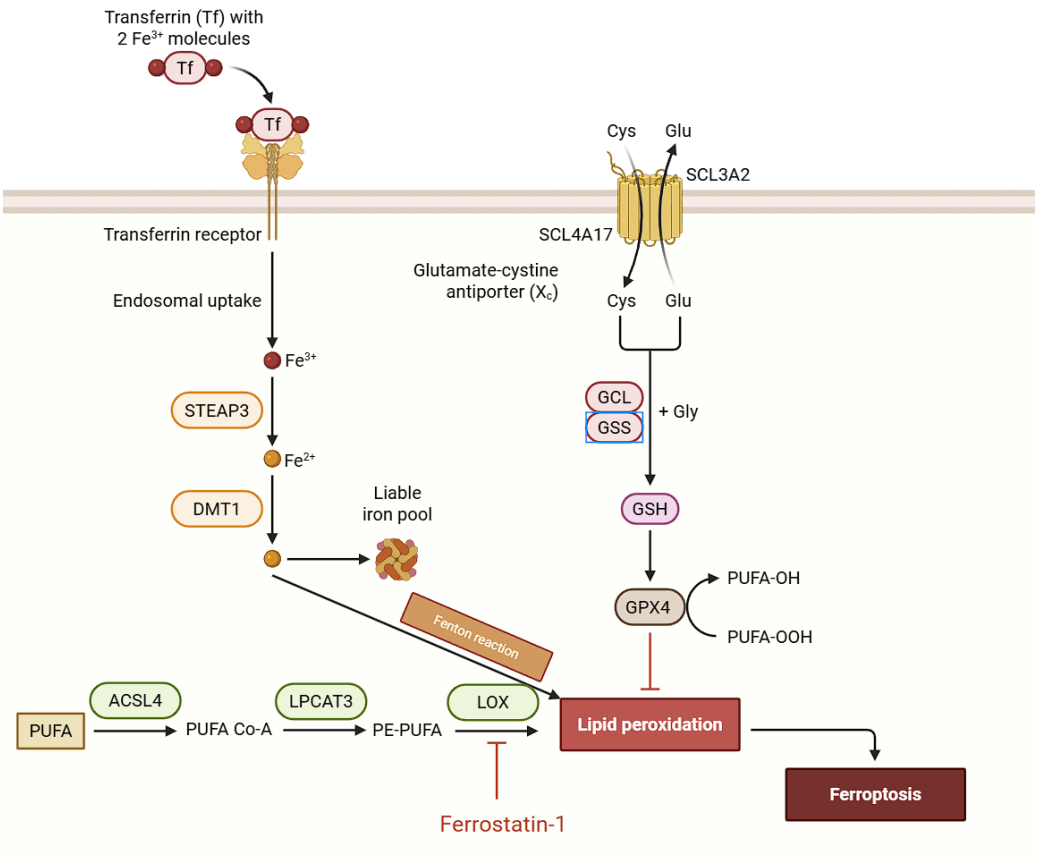

Figure 3: Brief summary of mechanisms regulating ferroptosis

This diagram illustrates the molecular mechanisms regulating ferroptosis. Iron-bound transferrin (Tf-Fe^{3+}) is internalized via transferrin receptor-mediated endocytosis, where Fe^{3+} is reduced to Fe^{2+} by STEAP3 and transported into the cytosol by DMT1, contributing to the labile iron pool (LIP). Intracellular Fe^{2+} catalyzes the Fenton reaction, generating reactive oxygen species that initiate lipid peroxidation. Polyunsaturated fatty acids (PUFAs) are esterified by ACSL4 and LPCAT3 into membrane phospholipids (PE-PUFAs), which are oxidized by lipoxygenases (LOX) into lipid hydroperoxides (PUFA-OOH). The glutamate–cystine antiporter system Xc^- (comprising SLC7A11 and SLC3A2) imports cystine in exchange for glutamate. Cystine is reduced to cysteine and, along with glutamate and glycine, is used for glutathione (GSH) synthesis by GCL and GSS. GSH acts as a cofactor for glutathione peroxidase 4 (GPX4), which detoxifies lipid hydroperoxides to non-toxic lipid alcohols (PUFA-OH), thereby preventing lipid

peroxidation and subsequent ferroptosis. Inhibition of lipid peroxidation by Ferrostatin-1 suppresses ferroptotic cell death. Image adapted from Lugano, G. (2025) BioRender.

Skeletal muscle is the largest tissue compartment in individuals without obesity, accounting for approximately 30–40% of the total body weight in healthy adults [57]. Beyond its primary mechanical role of converting chemical energy into mechanical force, skeletal muscle also serves as a major iron storage site, with a total iron content comparable to that of the liver [58, 59]. Several studies have explored the association between ferroptosis and skeletal muscle disorders, particularly sarcopenia.

Sarcopenia is a complex geriatric syndrome characterized by age-related, involuntary loss of skeletal muscle mass and strength, which can begin as early as the fourth decade of life. Sarcopenia is marked by a progressive, linear decline in both muscle mass and strength, with studies suggesting that up to 50% of muscle mass may be lost by the age of 80 [60]. Several diagnostic criteria for sarcopenia vary by region and organization. For example, the European Working Group on Sarcopenia in Older People (EWGSOP2) provides widely used guidelines in Western countries, whereas the Asian Working Group for Sarcopenia (AWGS) 2019 guidelines are commonly used in Asia [61, 62]. Despite regional variations, all definitions consistently include assessments of muscle strength and mass as core components [62]. Sarcopenia significantly impairs quality of life and is associated with increased morbidity and mortality [63].

In this context, ferroptosis appears to play a key role, particularly in satellite cell dysfunction and the loss of muscle fibers. In animal models of sarcopenia, such as

senescence-accelerated mouse prone 8 (SAMP8), researchers have observed elevated iron levels and increased ferroptosis markers in the skeletal muscle compared to younger controls. These findings were accompanied by a reduction in muscle mass and fiber size [64]. Iron overload in skeletal muscles promotes a pro-oxidative environment that contributes to muscle dysfunction and atrophy, both of which are hallmarks of aging muscle. A decline in transferrin receptor 1 (Tfr1) expression impairs skeletal muscle regeneration, leading to an increased labile iron pool (LIP), activation of unsaturated fatty acid biosynthesis, and decreased levels of GPX4 and Nrf2 in aging mice [65, 66]. Additionally, elevated iron levels have been shown to inhibit myoblast differentiation [67]. In my laboratory (Sweeney Lab), we have previously investigated the role of ferroptosis in the skeletal muscle. In one of our initial studies, electrical stimulation of skeletal muscle increased nitric oxide production, which subsequently elevated reactive oxygen species (ROS) generation, a hallmark of ferroptosis [68].

These findings provide compelling evidence of a direct link between ferroptosis and sarcopenic changes. Currently, treatment options for sarcopenia are primarily supportive, focusing on resistance exercise and protein supplementation [69]. However, specific pharmacological therapies targeting the underlying mechanisms of sarcopenia, including ferroptosis, remain under development.

1.3 ALY688 as a potent adiponectin receptor agonist

Adiponectin is a hormone secreted by the adipose tissue. It was identified in 1995 by Dr. Philipp E. Scherer [48]. Its structure varies depending on the species.

Human adiponectin is composed of 244 amino acid polypeptides and is formed into single-chain trimers, including a variable N-terminal domain, a collagen domain, and a C-terminal globular domain homologous to the immune complement C1q [70]. There are three forms of adiponectin oligomers that circulate in the plasma, separated by molecular weight: low molecular weight (LMW), medium (MMW), and high molecular weight (HMW). Finally, the monomer of adiponectin is a globular domain (gAd). Each form has a different property to attach to the adiponectin receptor and activate the cascade mechanism [52, 71]. Adiponectin exerts its biological effects through two primary membrane receptors, adiponectin receptor 1 and 2 (AdipoR1 and AdipoR2), which were discovered in 2003 by Dr. Toshimasa Yamauchi [72]. AdipoR1 demonstrates a high affinity for globular adiponectin and a low affinity for full-length adiponectin, with predominant expression in the skeletal muscle, while AdipoR2 shows an intermediate affinity for both globular and full-length HMW adiponectin forms and is primarily expressed in the liver and adipose tissue [73-75]. Both receptors also have adaptor proteins called Adaptor protein, Phospho-tyrosine interacting with pH domain Leucine zipper-1 (APPL-1) and APPL-2, corresponding to AdipoR1 and AdipoR2, respectively [76]. These adaptors can integrate signals from multiple pathways via localization to specific endosomal compartments and through multiple protein-protein interactions [77]. Upon adiponectin binding to AdipoR1 in skeletal muscle, an activation cascade of signals is initiated, leading to the activation of AMP-activated protein kinase (AMPK) via phosphorylation at Thr172 [78]. Previous studies have shown that adiponectin enhances insulin signaling pathway activation, including increased phosphorylation of key insulin signaling molecules such as insulin receptor substrate-1 (IRS1) and protein

kinase B (Akt) [79]. It also helps mitochondrial biogenesis, which reduces the production of reactive oxygen species [80]. Based on the knowledge of these mechanisms, many researchers have found a link between adiponectin and therapies for diseases, including cardiovascular disease, insulin resistance, and skeletal muscle diseases [49-53]. For example, Duchenne Muscular Dystrophy (DMD) is an X-linked genetic disorder that results in weakness due to muscle degeneration [81]. Adiponectin deficiency exacerbates dystrophic features in DMD, whereas local administration of adiponectin gene therapy lowers oxidative stress markers (e.g., TNF-α and IL-17A) and upregulates myogenic regulators, such as myosin heavy chain. From these mechanisms, muscle architecture is preserved during the early stages of the disease [82, 83]. The relationship between sarcopenia and adiponectin is complicated and paradoxical compared to other muscle diseases. Meta-analyses of cross-sectional studies comparing serum adiponectin levels between patients with sarcopenia and controls have revealed that sarcopenic participants had significantly higher levels of adiponectin [84]. However, this paradox may stem from two interrelated mechanisms. First, adiponectin resistance, driven by chronic inflammation through cytokines such as TNF-α and IL-6, leads to the downregulation of AdipoR1 and AdipoR2 receptors, thereby impairing adiponectin-mediated anabolic signaling [85]. Second, compensatory secretion occurs as part of adipose-muscle crosstalk during aging, in which adiponectin levels increase to mitigate insulin resistance and intramuscular lipid accumulation. However, this increase is often inadequate to restore proper metabolic function, contributing to the persistence of metabolic dysfunction [84].

ALY688 is a small synthetic peptide analog of adiponectin (ALY688; H-DAsn-Ile-Pro-Nva-Leu-Tyr-DSer-Phe-Ala-DSer-NH2) [86]. It has been shown to activate adiponectin-specific signaling downstream of both AdipoR1 and AdipoR2 receptors [86, 87]. This peptide has a better affinity for AdipoR1/2 and is more resistant to proteolytic degradation than gAd [54]. ALY688 also has a better safety profile than other adiponectin agonists, such as AdipoRon, which has failed toxicology tests in animal models [88, 89]. ALY688 also attenuates inflammation in various inflammatory disorders, such as dry eye and liver diseases [86, 90].. Furthermore, in the DMD model, ALY688 attenuates fibrosis and atrophy of skeletal muscle in mice and slows the progression of DMD complications, including cognitive impairment and diaphragm atrophy [50, 87, 90]. A meta-analysis showed increased adiponectin levels in patients with sarcopenia [84]. These findings support the concept that endogenous adiponectin signaling is impaired in sarcopenia, creating a therapeutic opportunity for receptor agonists that can bypass the resistance mechanisms.

1.4 Nrf 2 and its protective effect against ferroptosis

Nuclear factor erythroid 2–related factor 2 (Nrf2) is a transcription factor composed of seven functional domains, known as Neh domains (Nrf2-ECH homology domains). Each domain plays a distinct role in the regulation of Nrf2 activity and function. The Neh1, Neh4, and Neh5 domains bind to antioxidant response elements (AREs) through different mechanisms. Neh1 contains CNC/bZIP (Cap ‘n’ Collar/basic leucine zipper) motifs that allow Nrf2 to form heterodimers with small musculoaponeurotic fibrosarcoma (sMAF) proteins, enabling its binding to AREs [91,

92]. Neh4 and Neh5, on the other hand, interact with CREB-binding protein (CBP) to enhance transcriptional activation by facilitating ARE binding [93]. The Neh2 and Neh6 domains are central to the regulation and degradation of Nrf2. The Neh2 domain binds to the DC domain of Kelch-like ECH-associated protein 1 (Keap1), promoting the ubiquitination and subsequent proteasomal degradation of Nrf2 under basal conditions. The Neh6 domain also contributes to degradation through a Keap1-independent pathway by interacting with β-TrCP, a component of the SCF E3 ubiquitin ligase complex [94, 95]. Lastly, the Neh3 domain binds to chromodomain helicase DNA-binding protein 6 (CHD6), a key factor involved in the oxidative DNA damage response, further extending Nrf2's role beyond antioxidant defense [96].

Nrf2 regulation primarily depends on its interaction with Keap1. Under normal conditions, Keap1 maintains low levels of Nrf2 by binding two molecules to the Neh2 domain of Nrf2 [95]. This complex subsequently recruits Cullin3 (Cul3) and Ring-Box 1 (Rbx1) to form a functional E3 ubiquitin ligase complex (Keap1-Cul3-Rbx1), which facilitates the ubiquitination and proteasomal degradation of Nrf2 [97]. During oxidative stress, Keap1 undergoes structural modification due to the oxidation of its reactive cysteine residues [98, 99] or through competitive binding with proteins such as p62 [100]. These modifications impair Keap1's ability to form the E3 ubiquitin ligase complex, resulting in Nrf2 stabilization [101]. Stabilized Nrf2 then translocates to the nucleus, where it forms heterodimers with small MAF proteins (sMAFs) and binds to the antioxidant response element (ARE), promoting the transcription of various antioxidant genes [101, 102].

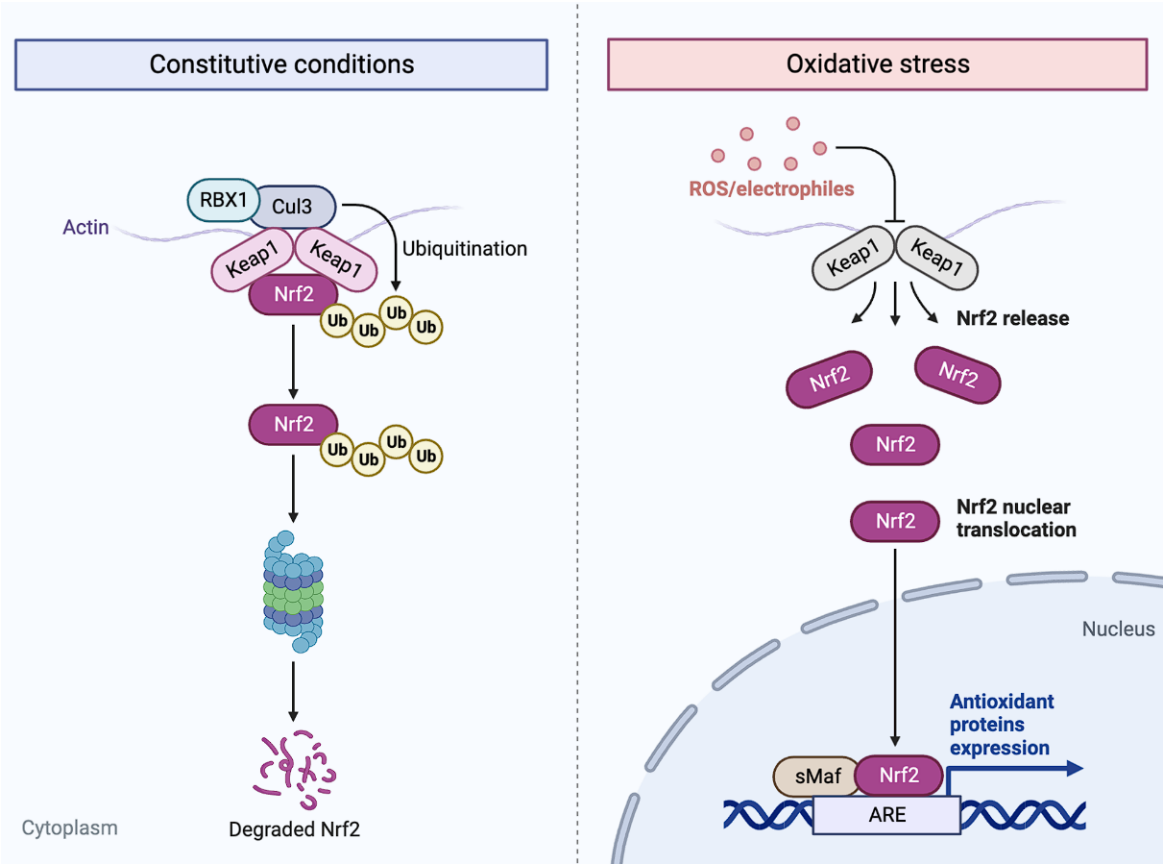

Figure 4: Nrf2 regulation under constitutive conditions and oxidative stress.

Schematic representation of Nrf2 regulation under constitutive and oxidative stress conditions. Under constitutive (basal) conditions (left panel), Nrf2 is bound by Keap1, which functions as a substrate adaptor for the Cul3-RBX1 E3 ubiquitin ligase complex, leading to Nrf2 ubiquitination and subsequent proteasomal degradation in the cytoplasm. In contrast, under oxidative stress (right panel), reactive oxygen species (ROS) or electrophiles modify cysteine residues on Keap1, inhibiting its ability to promote Nrf2 ubiquitination. Consequently, Nrf2 is stabilized and translocates into the nucleus, where it heterodimerizes with small Maf (sMaf) proteins and binds to antioxidant response elements (AREs) in the promoters of target genes, inducing the expression of antioxidant and cytoprotective proteins. Image retrieved from Ona, S. (2025) BioRender.

Sarcopenia is associated with age-related decline in Nrf2 expression. Studies in wild-type (WT) and Nrf2 knockout (KO) mice have demonstrated that Nrf2 deficiency accelerates frailty, reduces grip strength, and diminishes treadmill endurance by 20–24 months of age [103, 104]. In cancer-induced muscle wasting, Nrf2 dysregulation occurs through interleukin-1β (IL-1β)-mediated phosphorylation of p62 protein. Tumor-bearing Nrf2 KO mice show exacerbated muscle atrophy, whereas p62 activation restores extracellular superoxide dismutase (EcSOD) expression and mitigates oxidative damage [105]. Recent evidence has revealed direct molecular interactions between adiponectin and the Nrf2 pathway, particularly via adiponectin receptor 1 (AdipoR1), which plays a key role in activating Nrf2. One study demonstrated that globular adiponectin, the active form of adiponectin, activates Nrf2 via the p21/p62/Nrf2 signaling axis. Knocking down p62 or p21 significantly reduced Nrf2 activation by globular adiponectin [106]. Another study involving hepatocarcinoma cells offered insight into the rationale for administering chemotherapy prior to radiation therapy, a sequence that previously lacked a mechanistic explanation. The study found that radiation therapy induced AdipoR1 expression, which subsequently activated Nrf2. This activation leads to the upregulation of system Xc^--related genes, including SLC7A11 and GSH, both of which are essential for cellular antioxidant defense [107].

Chapter 2: *"The adiponectin receptor agonist ALY688 protects against iron-induced ferroptosis via Nrf2 activation in skeletal muscle"*

2.1 Abstract

Ferroptosis is a form of regulated cell death marked by lipid peroxidation and is increasingly relevant in muscle degeneration. Arachidonic acid (AA), a polyunsaturated fatty acid, enhances susceptibility to iron overload (IO)-induced ferroptosis. This study investigated the protective role of ALY688, an adiponectin receptor agonist, in skeletal muscle cells under ferroptotic stress. In L6 cells, AA and IO co-treatment led to a 2-fold increase in oxidative stress (p<0.001), accompanied by significant elevations in total and mitochondrial lipid peroxidation (p<0.0001). Similar effects were observed in iPSC-derived myogenic progenitors (iPSC-MPs). ALY688 significantly reduced ROS and lipid peroxidation in both cell types (p<0.01) and protected against ferroptotic cell death (p<0.01, p<0.0001). Notably, ALY688 activated the Nrf2 antioxidant pathway, as evidenced by upregulation of downstream genes, including those in the GPX4 system ($p<0.05$). The cytoprotective effect of ALY688 was abolished by ML385, an Nrf2 inhibitor (p<0.001), confirming Nrf2 dependency. These findings reveal that AA sensitizes skeletal muscle cells to ferroptosis and that ALY688 mitigates this process via Nrf2 activation, suggesting its therapeutic potential in oxidative stress–related muscle degeneration.

2.2 Introduction

Metabolic syndrome (MetS) is a clinical condition diagnosed when an individual meets at least three of five criteria including (1) abdominal obesity, defined as a waist circumference >102 cm (40 in) in men or >88 cm (35 in) in women; (2) elevated triglycerides (≥150 mg/dL); (3) reduced HDL cholesterol (<40 mg/dL in men or <50 mg/dL in women); (4) hypertension (blood pressure ≥130/85 mmHg); and (5) elevated fasting glucose (≥100 mg/dL) [1, 5]. MetS presents significant health challenges, ranging from individual complications to broader public health impacts. In Canada, the prevalence of MetS is estimated to be approximately 14.9% [7]. The complications associated with MetS are well established and include an increased risk of developing cardiovascular disease and type 2 diabetes [1].

However, emerging evidence suggests a link between metabolic syndrome (MetS) and iron metabolism. The term metabolic hyperferritinemia (MHF) has been introduced to describe a condition in which individuals with iron overload develop insulin resistance, and conversely, patients with metabolic disorders frequently exhibit elevated ferritin levels [14, 21]. Excess iron tends to accumulate in various organs, particularly the liver and heart, leading to progressive organ damage. In the advanced stages of MHF, where organ dysfunction is evident, the condition is referred to as dysmetabolic iron overload syndrome (DIOS) [15, 16]. Skeletal muscle accounts for approximately 30–40% of the total body weight in healthy adults [57]. In a mouse model, iron overload was found to lead to muscle atrophy and progressive loss of muscle mass [25]. Moreover, several clinical studies have reported that individuals with both sarcopenia and metabolic syndrome often exhibit iron overload [23, 24, 26], suggesting a potential association

between the two. These findings imply that conditions such as MHF and DIOS may contribute to the development or progression of sarcopenia.

Sarcopenia is characterized by a progressive loss of muscle mass and strength [60]. Recent studies have identified a potential link between ferroptosis, a form of regulated cell death driven by iron overload and lipid peroxidation, and sarcopenia development. In my laboratory (Sweeney Lab), we have previously investigated the role of ferroptosis in the skeletal muscle. In our laboratory (Sweeney Lab), we have previously explored the role of ferroptosis in the skeletal muscle. One of our initial studies demonstrated that electrical stimulation of skeletal muscle increased nitric oxide production, which in turn led to elevated reactive oxygen species (ROS) generation, a hallmark of ferroptotic stress [68]. Furthermore, in animal models of sarcopenia, such as senescence-accelerated mouse prone 8 (SAMP8), researchers observed elevated iron levels and increased expression of ferroptosis markers in the skeletal muscle compared to age-matched younger controls. These molecular changes are accompanied by a measurable reduction in muscle mass and fiber size [64]. These findings provide compelling evidence of a direct link between ferroptosis and sarcopenic changes. Currently, treatment options for sarcopenia are primarily supportive, focusing on resistance exercise and protein supplementation [69]. However, targeted pharmacological therapies aimed at molecular mechanisms such as ferroptosis are still under investigation.

ALY688 is a small synthetic peptide analog of adiponectin (ALY688; H-DAsn-Ile-Pro-Nva-Leu-Tyr-DSer-Phe-Ala-DSer-NH2) [86]. This peptide has a better affinity for AdipoR1/2 and is more resistant to proteolytic degradation than natural adiponectin or

other synthesis adiponectin agonist [54]. ALY688 has been shown to attenuate fibrosis and muscle atrophy in skeletal muscle and to slow the progression of Duchenne muscular dystrophy (DMD) and related complications, including cognitive impairment and diaphragm atrophy, in mouse models [50, 87, 90]. It is also known to activate signaling pathways such as AMPK, PGC-1α, and other antioxidant-related mechanisms [108].

Nuclear factor erythroid 2–related factor 2 (Nrf2) is a transcription factor that regulates genes involved in the antioxidant defense system. Recent study involving hepatocarcinoma cells offered insight into the rationale for administering chemotherapy prior to radiation therapy, a sequence that previously lacked a mechanistic explanation. The study found that radiation therapy induced AdipoR1 expression, which subsequently activated Nrf2. This activation leads to the upregulation of system Xc^--related genes, including SLC7A11 and GSH, both of which are essential for cellular antioxidant defense [107]. These findings support a mechanistic link between ALY688, Nrf2 activation, and protection against ferroptosis, offering a potential explanation for its cytoprotective effects in skeletal muscle.

This study aimed to investigate the protective effects of ALY688 against ferroptosis in skeletal muscle cells. Existing literature indicates that the activation of adiponectin receptors stimulates Nrf2, which subsequently inhibits ferroptosis by upregulating system Xc^--related genes [55, 107]. In this study, ALY688 was used to activate adiponectin receptors, thereby promoting Nrf2 signaling and protecting skeletal muscle cells from ferroptotic cell death.

I hypothesized that alterations in lipid composition in skeletal muscle cells increase their susceptibility to ferroptosis in the presence of iron overload and that ALY688 can protect cells from ferroptosis through Nrf2 activation.

To test this hypothesis, I addressed the following research aims.

Aim 1: Does arachidonic acid (AA) increase susceptibility to iron-induced ferroptosis in skeletal muscle cells?

Aim 2: Does ALY688 attenuate iron-induced ferroptosis in the presence of AA?

Aim 3: Is ALY688's effect mediated via Nrf2 signaling?

2.3 Materials and methods

Cell culture and maintenance of L6 skeletal muscle cells

The L6 rat skeletal muscle cell line was grown in alpha-minimum essential medium (AMEM) (Wisent, #310-010 CL) supplemented with 10% fetal bovine serum (FBS) (Thermo, # A3160702) and 1% antibiotic/antimycotic (Gibco, #15240062) at 37°C with 95% air and 5% CO2. For arachidonic acid treatment, L6 cells were treated with arachidonic acid diluted in AMEM containing 2% FBS and 2% bovine serum albumin (BSA). For iron overload, L6 cells were treated with iron diluted in AMEM containing 0.5% FBS.

The iPSCs line pgpc14 [109] was seeded on Matrigel-coated plates at a density of 31,000 cells/cm2, differentiated into myogenic progenitors (MPs), passaged, and expanded following the manufacturer's protocol (STEMCELL Technologies, #100-0151).

For passage #5 or higher, iPSC-MPs were seeded on Matrigel-coated surfaces at a density of 5,000-10,000 cells/cm2 in skeletal muscle growth media (Lonza, #CC-3245). Upon reaching 80% confluence, approximately every 3 days, iPSC-MPs were detached with TrypLE express (Thermo, #12605010) diluted 1:1 with PBS. All experiments were performed using cells below passage 20. Where indicated, iPSC-MPs (below passage 5) were differentiated into myotubes using the MyoCult™ Differentiation Kit (STEMCELL Technologies, #05965). Serum-free low-glucose DMEM was used for all treatments in iPSC-MPs or myotubes.

Expanding Escherichia coli cells with pREP-8xARE-GFP-SV40-BFP plasmid

L6 Nrf2 reporter cells were generated using the pREP-8xARE-GFP-SV40-BFP plasmid (Addgene #134910). Prior to transfection, wild-type L6 (WT) cells were cultured in a T75 flask until they reached approximately 90% confluency. The plasmid was transformed into Escherichia coli (*E. coli*) and stored in a Luria Broth (LB) agar stab. To amplify the bacteria, the preserved *E. coli* was streaked onto LB agar plates. LB agar was prepared by mixing 25 g of LB powder (Invitrogen, #12795027), 12.5 g of agarose powder (BioShop, #AGA001.100), and 500 mL of distilled water. The mixture was autoclaved before pouring it into the plates. After cooling, ampicillin (BioShop, #AMP201.100) was added to the media. Using aseptic technique, the *E. coli* containing the plasmid was spread onto the plates and incubated at 37°C for 24 hours. A single colony was selected and inoculated into LB liquid culture to allow sufficient bacterial growth for plasmid DNA purification. Liquid LB medium was prepared using 25 g of LB powder (Invitrogen, #12795027) dissolved in 1 L of distilled water. The selected *E. coli*

colony was transferred into the medium and incubated at 37°C for 24 h with shaking at 250 RPM.

Plasmid purification

Transformed E. coli culture (12 mL) was centrifuged at 4,000 × g for 10 min. After discarding the supernatant, the resulting bacterial pellet was resuspended in lysis and wash buffers provided by the PureLink™ HiPure Plasmid Miniprep Kit (Invitrogen, #K2100-02). Subsequent plasmid purification steps were performed according to the manufacturer's protocol. DNA concentrations were quantified using a plate reader, and the purified plasmids were stored at − 80°C for future use.

Making L6-Nrf2 reporter cell

Prior to transfection, wild-type L6 (WT) cells were cultured in a 6-well plate until they reached approximately 90% confluency. Two distinct mixtures were prepared before being added to the L6 WT cells: a lipofectamine mixture and a plasmid mixture. Various ratios of these mixtures were tested to determine the most effective transfection condition. The DNA-to-Lipofectamine ratios tested were 1:0.75, 1:1, and 1:1.5. Each lipofectamine mixture was prepared using Lipofectamine™ 3000 (Invitrogen, #L3000001) and Opti-MEM™ (Gibco, #31985062) as follows: 1:0.75 ratio: 7.5 µL Lipofectamine 3000 + 42.5 µL Opti-MEM, 1:1 ratio: 10 µL Lipofectamine 3000 + 40 µL Opti-MEM, and 1:1.5 ratio: 15 µL Lipofectamine 3000 + 35 µL Opti-MEM. The plasmid mixture remained consistent across all conditions and consisted of 6.5 µL purified

plasmid DNA, 20 µL P3000™ Enhancer Reagent (Invitrogen, #L3000001), and 23.45 µL Opti-MEM. Equal volumes of Lipofectamine and plasmid mixtures were gently combined and incubated at room temperature for 15 min to allow complex formation. L6 WT cells were then treated with 50 µL of the combined transfection complex in 1,000 µL of 10% AMEM containing 10% FBS. Cells were incubated at 37°C in an atmosphere of 95% air and 5% CO_2 for 24 h. On Day 2, transfected cells were selected using puromycin (Gibco, #A1113803) at a concentration of 1 µg/mL. A second round of puromycin selection was performed seven days later to ensure stable transfection.

Chemicals

The chemicals used included iron (II) sulfate heptahydrate (FeSO4) (Bioshop, #FER005.250), arachidonic acid (Sigma-Aldrich, #10931-1G), and ferrostatin-1 (Sigma-Aldrich, #SML0543-5G)

CellROX™ Deep Red Reagent kit, for oxidative stress detection

The CellROX™ Deep Red Reagent kit (Invitrogen, # C10422) was used to measure reactive oxygen species (ROS) inside the cells. This reagent is non-fluorescent in its reduced state. ROS can oxidize and emit fluorescence at 665 nm, which can be detected using fluorescent imaging. L6 WT cells were treated with 80µM arachidonic acid (AA) for 24h, followed by pre-treatment with ALY688 for 30 min and then 100µM FeSO4 for 24h (IO). Imaging was performed using a Nikon A1 confocal

microscope in a 5% CO2 live-cell chamber. The results were quantified using the ImageJ software.

Image-iT® Lipid peroxidation assay

The Image-iT® Lipid Peroxidation Kit (Invitrogen, #C10445) was used to measure total lipid peroxidation in L6 WT cells treated with 80μM arachidonic acid (AA) for 24h, followed by pre-treatment with 1μM Ferostatin-1 or ALY688 for 30 min and then 100μM or 250μM FeSO4 for 24h. The assay is based on the oxidation of lipids in cells, which oxidizes fluorescence to shift from red to green. Therefore, the appearance of green fluorescence indicates lipid peroxidation. After completing the treatments, L6 WT cells were stained with Image-iT® lipid peroxidation kit mixed with alpha-minimum essential medium without Phenol Red medium (AMEM) (Wisent, # 310-021 CL) and incubated for 30 min at 37°C. The measurements were done on Imaging was performed using a Nikon A1 confocal microscope in a 5% CO2 live-cell chamber. The results were quantified using the ImageJ software.

Mitochondria lipid peroxidation probe

MitoCLox is a mitochondria-targeted fluorescence probe (Lumiprobe, #3549-500ug) that specifically binds to cardiolipin, a mitochondria-specific phospholipid. When it reacts with cardiolipin, the probe is oxidized, which increases the fluorescence emission at 520 nm and decreases the fluorescence at 590 nm (the signal shifts from red to green). This probe was used for L6 WT cells treated with 80μM arachidonic acid (AA) for 24h, followed by pre-treatment with 1μM Ferostatin-1 or ALY688 for 30 min and

then 100μM $FeSO_4$ for 24h (IO). The measurements were performed using a Nikon A1 confocal microscope in a 5% CO_2 live-cell chamber. The results were quantified using the ImageJ software.

Western blotting

L6 WT cells were grown to approximately 70% confluency in 6-well plates. Then, they were treated with 80μM arachidonic acid (AA) for 24h, followed by $FeSO_4$ for 24h (IO) 100μM. All samples were washed with PBS (Gibco, #10010049) and incubated with lysis buffer for 20 min. The stock lysis components consisted of 50mM Tris, 0.1% SDS, and 30% glycerol, which were complemented with Pierce™ protease and phosphatase inhibitor mini tablets (Thermo Scientific, #A32959) [consisting of Aprotinin, Bestatin, E-64, Leupeptin, Sodium fluoride, sodium orthovanadate, sodium pyrophosphate, and β-glycerophosphate], 10% β-mercaptoethanol, and bromothymol blue was added to the stock lysis buffer with the protease inhibitor cocktail. Each sample was vortexed for 1 min for further lysis. The cells were centrifuged at 10,000 RPM for 10 min at 4°C before denaturation at 95°C for 5 min. The lysates were run on 10% SDS-PAGE gels at 90 V for 2 h. The gels were transferred to a polyvinylidene difluoride (PVDF) membrane (BioRad, #162-0177) at 120 V for 1.5 h. The PVDF membrane was blocked with 3% bovine serum albumin (BSA) (Bioshop, #ALB001.1) for 1 h. The membrane was incubated overnight at 4°C with primary antibodies including glutathione peroxidase 4 (GPX4)(Abcam, #AB125066), dihydroorotate dehydrogenase (DHODH) (Cell Signaling, #5114S), ferroptosis suppressor protein 1 (FSP1) (Santa Cruz; #sc-377120 hrp), and glyceraldehyde 3-phosphate dehydrogenase (GAPDH) (Cell Signaling, #2118). GPX4 is

the main protective factor against ferroptosis. However, DHODH and FSP1 are representative of parallel pathways that counteract ferroptosis. After primary antibody incubation, the PVDF membrane was washed three times with wash buffer before incubation with secondary antibody at 1:5000 dilution (anti-rabbit immunoglobulin G horseradish peroxidase-conjugated antibody) (Cell Signaling, #7074S) at room temperature for 1 h. The cells were then washed three times with washing buffer. Finally, the membranes were washed with Clarity Western ECL Substrate solution (BioRad, #1705061). The film was visualized using X-ray film (Diamed, #DIAFILM810-LITE) development Western blot bands were quantified using ImageJ software and normalized to GAPDH.

Lactate dehydrogenase (LDH) assay

An LDH assay (G-Biosciences, #786-210) was used to determine the cytolysis and cellular cytotoxicity of L6 cells. After the treatments, 50µL of culture media was added to a new 96-well plate with 50µL of LDH reaction mix from the kit. The plate was incubated for 30 min at room temperature and covered with aluminum foil. The samples were measured using a plate reader at wavelengths 490 nm and 680 nm. The quantification used by subtraction the of 680 nm from the 490 nm value, and then normalized by calculating the fold change compared to the control.

ReadyProbes™ Cell Viability Imaging Kit, Blue/Green

Readyprobe (Invitrogen, #R37609) is a fluorescence-based assay that works by detecting percentage of live cells. This kit comprises NucBlue® Live reagent (Hoechst' #33342) and NucGreen® Dead reagent. NucGreen® Dead reagent can infiltrate dead cells, which have decreased cell membrane integrity. Both reagents can be detected using fluorescence microscopy. L6 WT in 96 well plate were treated with 80μM arachidonic acid (AA) for 24h, followed by pre-treatment with 1μM Ferostatin-1 or ALY688 for 30 min and then 100μM or 250μM $FeSO_4$ for 24h. One drop of each reagent was applied to alpha-minimum essential medium (AMEM) 1mL. The cells were then incubated at 37°C for 30 min. Cells were imaged using an EVOS fluorescent microscope. The results were quantified using ImageJ software, and the percentage of dead cells was calculated by dividing the number of nonviable cells (green) by the total number of cells (blue).

GSH/GSSG-Glo™ Assay

The GSH/GSSG-Glo™ Assay Kit (Promega #V6911) was used to measure intracellular glutathione (GSH) and oxidized glutathione (GSSG) levels in L6 cells. After treatment, the cell media were removed. Subsequently, 50 μL of the prepared cell lysate was mixed with either Total or Oxidized Glutathione Reagent for 5 min on a shaker. Subsequently, 50 μL of Luciferin Generation Reagent was added to the wells and incubated at room temperature for 15 min. Finally, the plate was read using a plate reader for luminescence.

Statistical analysis

Data are presented as mean ±SEM. The statistical significance between the treatment groups was calculated using a paired t-test when comparing two groups. For comparisons of more than two groups and one-Way ANOVA were used. A *p-value* < 0.05 was considered statistically significant and plotted using GraphPad Prism 10.

2.4 Results

ALY688 Attenuates Oxidative Stress Induced by Arachidonic Acid and Iron in L6WT Cells

Polyunsaturated fatty acids (PUFAs) are well-established contributors to ferroptosis, promoting oxidative stress and lipid peroxidation [38]. To investigate this process in L6 skeletal muscle cells, the cells were treated with 80 μM AA for 24 h, followed by 100 μM $FeSO_4$ (IO) for an additional 24 h. In the ALY688 treatment group, ALY688 300nM was administered as a 30-minute pre-treatment prior to iron exposure. After treatment, CellROX™ Deep Red Reagent was used to monitor oxidative stress in live cells. This dye is cell-permeable and remains non-fluorescent in its reduced state. Upon oxidation by reactive oxygen species (ROS), such as hydroxyl radicals and superoxide anions, the probe undergoes a structural transformation that produces intense near-infrared fluorescence, with excitation/emission maxima of 644/665 nm [110].

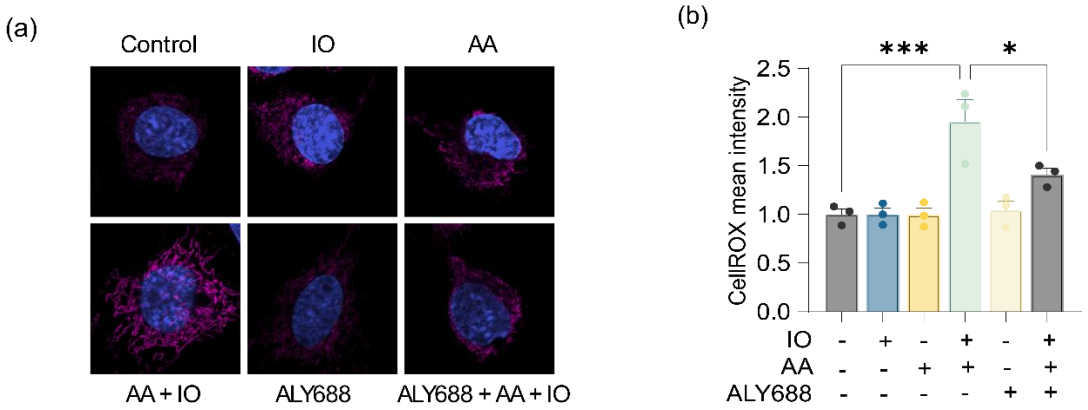

Figure 5: ALY688 Attenuates Oxidative Stress Induced by Arachidonic Acid and Iron in L6WT Cells

*Oxidative stress in L6 cells was measured using CellROX™ Deep Red Reagent. Representative images of wild-type L6 (L6WT) cells stained with DAPI (blue) and CellROX (purple) are shown in **(a)**. L6WT cells were treated with 80μM arachidonic acid (AA) for 24h, followed by pre-treatment with ALY688 300 nM for 30 min and then exposed to 100μM $FeSO_4$ for 24h (IO) **(b)**. Data are presented as mean ± SEM. *p<0.05, ***p<0.001 (n=3). (one-way ANOVA with multiple comparisons)*

The results showed that treatment with either iron overload (IO) or arachidonic acid (AA) alone did not significantly increase oxidative stress compared to that in the control group. However, the combination of AA and IO significantly increased oxidative stress. Pre-treatment with ALY688 effectively reduced oxidative stress induced by the combined AA and IO treatment, suggesting its protective effect (Figure 5 a, b). Based on these findings, I decided to further investigate the specific type of oxidative stress associated with ferroptosis, particularly lipid peroxidation.

ALY688 Attenuates Lipid Peroxidation Induced by Arachidonic Acid and Iron in L6 Cells.

After confirming that the IO combination increased oxidative stress, Image-iT™ Lipid Peroxidation probes were used to assess total lipid peroxidation in the cells. These probes function by detecting shifts in fluorescence emission between the reduced and oxidized states of the probe. In the reduced state, the probe emitted red fluorescence with a peak at approximately 590 nm (excitation/emission: 581/591 nm). Upon oxidation by lipid hydroperoxides, reactive intermediates produced during lipid peroxidation, the probe undergoes a fluorescence shift to ~510 nm, resulting in green fluorescence [111]. Before testing, L6 wild-type (L6WT) cells were treated under the same conditions as

those in the previous oxidative stress experiment. However, the concentration of $FeSO_4$ was increased to 250 µM to determine whether a higher iron concentration alone could induce lipid peroxidation. In addition, Ferrostatin-1 (Fer-1), a synthetic small molecule known as a potent and selective inhibitor of ferroptosis [112], was included as a positive control in this experiment. The goal was to compare the effects of ALY688 and ferrostatin-1 in reducing lipid peroxidation. If ALY688 shows a similar reduction in lipid peroxidation, it may suggest that ALY688 protects against ferroptosis. After obtaining the images, the mean fluorescence intensity of the green (oxidized probe indicating lipid peroxidation) and red channels (reduced) was quantified.

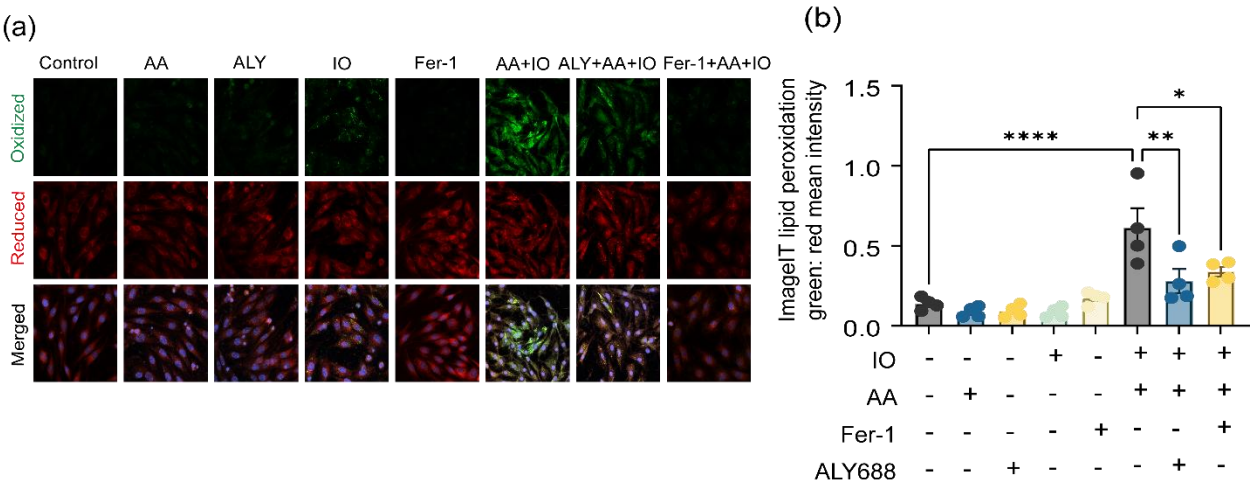

Figure 6 : ALY688 Attenuates Lipid Peroxidation Induced by Arachidonic Acid and Iron in L6 Cells.

*Lipid peroxidation in L6 cells was assessed using the Image-iT™ Lipid Peroxidation Probe, and fluorescence signals were detected using confocal fluorescence microscopy. Representative image of Image-iT™ lipid peroxidation probe staining of wild-type L6 (L6WT) cells **(a)**. L6WT cells were treated with 80 µM arachidonic acid (AA) for 24 h, followed by a 30-minute pre-treatment with either 1 µM Ferrostatin-1 (Fer-1) or ALY688, and then exposed to 100 µM $FeSO_4$ (IO100µM) for an additional 24 h. (IO) **(b)**. The intensity of lipid peroxidation was quantified and expressed as the ratio of oxidized (green) to reduced (red) fluorescence. Data are presented as*

*mean ± SEM. *p<0.05, **p<0.01, ****p<0.0001 (n=4). (one-way ANOVA with multiple comparisons)*

The results showed that individual treatments with 100 μM $FeSO_4$ (IO100), or arachidonic acid (AA) did not significantly increase lipid peroxidation compared to that in the control. However, the combination of IO and AA significantly increased lipid peroxidation at both iron concentrations (Figure 6 b). Based on these findings, 100 μM $FeSO_4$ was used as the minimum effective concentration that induced lipid peroxidation, which may also imply ferroptosis involvement. Pre-treatment with ALY688 or Ferrostatin-1 (Fer-1) effectively prevented the increase in lipid peroxidation, consistent with the results observed for oxidative stress (Figure 6 a, b). This suggests that lipid peroxidation is a major contributor to oxidative stress under AA + iron treatment conditions and that ALY688 exhibits protective properties similar to those of ferrostatin-1 against lipid peroxidation.

Does the AA combined with iron treatment induce mitochondria lipid peroxidation?

Mitochondria were chosen for further examination of lipid peroxidation because they are the primary source of reactive oxygen species (ROS), which are byproducts of the electron transport chain during cellular respiration [113]. In addition, the inner mitochondrial membrane is rich in polyunsaturated fatty acids (PUFAs), particularly cardiolipin, which renders it highly susceptible to oxidative damage. Disruption of mitochondrial function by cytosolic ROS or iron-dependent Fenton reactions can initiate widespread lipid peroxidation, ultimately leading to ferroptosis [114]. To detect

mitochondrial lipid peroxidation, mitoCLox was used, which is a specialized probe structurally similar to the general lipid peroxidation probe but modified to target mitochondria. It contains triphenylphosphonium (TPP), a well-established mitochondrial-targeting moiety. The positive charge of TPP promotes probe accumulation in the negatively charged mitochondrial matrix, driven by the mitochondrial membrane potential (MMP) [115]. The detection method was consistent with that of the Image-iT™ Lipid Peroxidation probe. MitoCLox emits red fluorescence in its reduced state (peak ~590 nm) and shifts to green fluorescence (~510 nm) upon oxidation, indicating lipid peroxidation. After image acquisition, the mean fluorescence intensity of the green (oxidized) and red (reduced) channels was quantified.

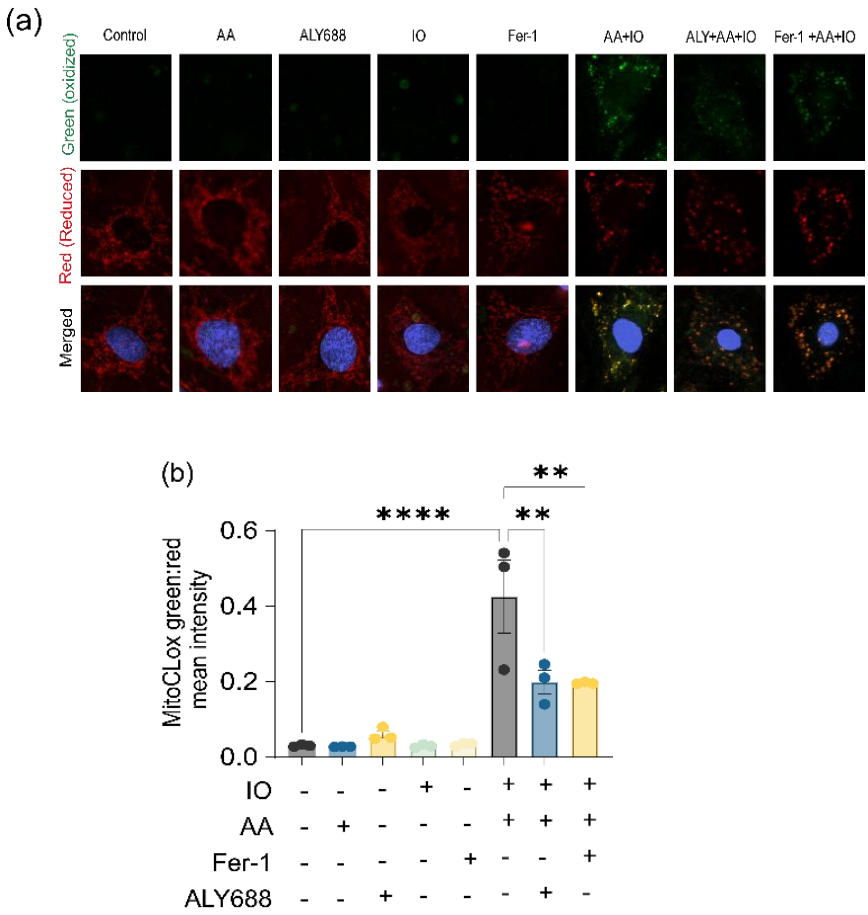

Figure 7: ALY688 Attenuates Mitochondrial Lipid Peroxidation Induced by Arachidonic Acid and Iron in L6WT Cells

Mitochondrial lipid peroxidation in wild-type L6 (L6WT) cells was assessed using MitoCLox, and fluorescence signals were detected using confocal fluorescence microscopy. Representative images of MitoCLox staining in L6WT cells are shown in ***(a)****. L6WT cells were treated with 80 µM arachidonic acid (AA) for 24 h, followed by a 30-minute pre-treatment with either 1 µM Ferrostatin-1 (Fer-1) or ALY688, and then exposed to 100 µM* $FeSO_4$ *(IO) for an additional 24 h. MitoCLox fluorescence intensity was quantified and expressed as the ratio of oxidized (green) to reduced (red) fluorescence* ***(b)****. Values are presented as the mean ± SEM. *p<0.05, **p<0.01, ***p<0.001, ****p<0.0001 (n=3). (one-way ANOVA with multiple comparisons)*

The results (Figure 7 a, b) were consistent with the total lipid peroxidation data obtained. Treatment with iron (IO) or arachidonic acid (AA) alone did not significantly increase mitochondrial lipid peroxidation compared to the control. However, the combination of AA and IO significantly increased mitochondrial lipid peroxidation levels. Importantly, ALY688 effectively prevented this increase, consistent with its protective effect observed in the total lipid peroxidation assay. These findings suggest that ALY688 limits lipid peroxidation within the mitochondria of L6 cells, thereby contributing to the reduction of overall cellular lipid peroxidation.

Combination treatment of AA and Iron altered anti-lipid peroxidation system.

As mentioned in the Introduction, disruption of the cellular antioxidant system is a key mechanism that contributes to ferroptosis and cell death. Among these systems, GPX4 plays a central role in the regulation of ferroptosis. GPX4 neutralizes lipid hydroperoxides by converting them into non-toxic lipid alcohols, thereby preventing lipid peroxidation-induced damage [81]. For GPX4 to function properly, it depends on the System Xc^-/GSH/GPX4 axis [116]. Cystine is imported into the cell via System Xc^-, where it is reduced to cysteine, a precursor for glutathione (GSH) synthesis. GSH donates electrons to GPX4, enabling the reduction of lipid hydroperoxides to lipid alcohols [117]. Although GPX4 represents the primary defense against ferroptosis, two additional GPX4-independent pathways, dihydroorotate dehydrogenase (DHODH) and Ferroptosis Suppressor Protein 1 (FSP1), have been identified as complementary mechanisms for lipid peroxide detoxification. DHODH is a mitochondrial inner membrane enzyme that is primarily involved in pyrimidine biosynthesis [118]. In the

context of ferroptosis, it plays a protective role by reducing ubiquinone (CoQ) to ubiquinol ($CoQH_2$). Ubiquinol donates electrons to detoxify lipid peroxyl radicals within the mitochondria, thereby interrupting lipid peroxidation chain reactions [119, 120]. In cancer cells, supplementation with dihydroorotate (a DHODH substrate) attenuates ferroptosis, whereas orotate (a DHODH product) exacerbates it, particularly in GPX4-deficient cells. These findings suggest that DHODH serves as a critical mitochondrial backup system when GPX4 activity becomes impaired [119]. FSP1 (Ferroptosis Suppressor Protein 1), previously known as AIFM2 (Apoptosis-Inducing Factor Mitochondria-Associated 2), was the first GPX4-independent ferroptosis suppressor to be identified [121]. It operates through the FSP1–CoQ10–NAD(P)H pathway [122], in which FSP1 reduces coenzyme Q10 (CoQ10) to ubiquinol ($CoQH_2$) using NADH as an electron donor. Ubiquinol functions as a lipid-soluble antioxidant, detoxifying lipid peroxides in both plasma and mitochondrial membranes, thereby halting the propagation of lipid peroxidation [119, 123].

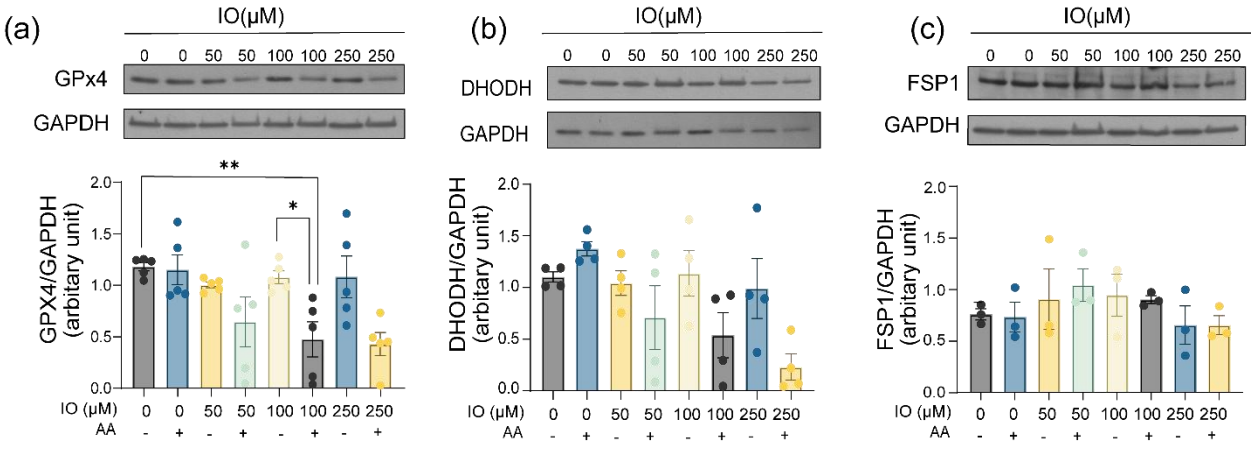

Figure 8: Combination treatment of AA and Iron altered anti-lipid peroxidation system.

L6 cells were treated with 80μM arachidonic acid (AA) for 24h followed by 24h of FeSO4 (IO 50-250μM). Western blot analysis of GPx4 (n=5), DHODH(n=4) and FSP1(n=3) are shown ***(a-c)****. Values are presented as mean ± SEM; *p<0.05, **p<0.01. (one-way ANOVA with multiple comparisons)*

The results showed that Individual treatment with either arachidonic acid (AA) or iron ($FeSO_4$, IO) did not significantly alter the expression levels of GPX4, DHODH, or FSP1 compared to the control. However, the combination of 100 μM IO with AA led to a significant decrease in GPX4 expression (Figure 8 a), suggesting the suppression of this key ferroptosis-regulating enzyme under co-treatment conditions. In contrast, the expression levels of DHODH (Figure 8 b) and FSP1 (Figure 8 c) remained unchanged, even under AA + IO co-treatment, indicating that these parallel anti-ferroptotic pathways were not significantly affected by this stress condition. Based on these findings, the data suggest that the GPX4 pathway is selectively impaired during AA- and iron-induced ferroptosis, whereas DHODH and FSP1 appear to remain stable. Therefore,

subsequent investigations will focus on cellular lipid peroxidation and further elucidation of the GPX4-dependent axis in this model.

ALY688 Attenuates Mitochondrial Lipid Peroxidation Induced by Arachidonic Acid and Iron in L6WT Cells

Induced pluripotent stem cells (iPSCs) are adult somatic cells that have been reprogrammed to regain pluripotency, similar to embryonic stem cells. This groundbreaking technology was first developed by Shinya Yamanaka and colleagues in 2006 [124]. Since then, iPSCs have been widely adapted for various applications, including drug development and patient-specific therapy.

In this study, induced pluripotent stem cell-derived myogenic progenitors (iPSC-MPs) were used to model the effects of iron and arachidonic acid (AA) treatment in human cells. This approach mimics the conditions that may contribute to metabolic hyperferritinemia (MHF). Myogenic progenitors, also known as myoblasts, represent the same developmental stage as L6 cells, which are a commonly used rat myoblast cell line. This parallel allows for cross-species comparisons and enhances the relevance of the findings in the context of human disease. In this study, mitochondrial lipid peroxidation was investigated in iPSC-MPs, similar to the assays performed in L6 cells, to evaluate whether ALY688 provides a protective effect against mitochondrial lipid peroxidation in iPSC-MPs.

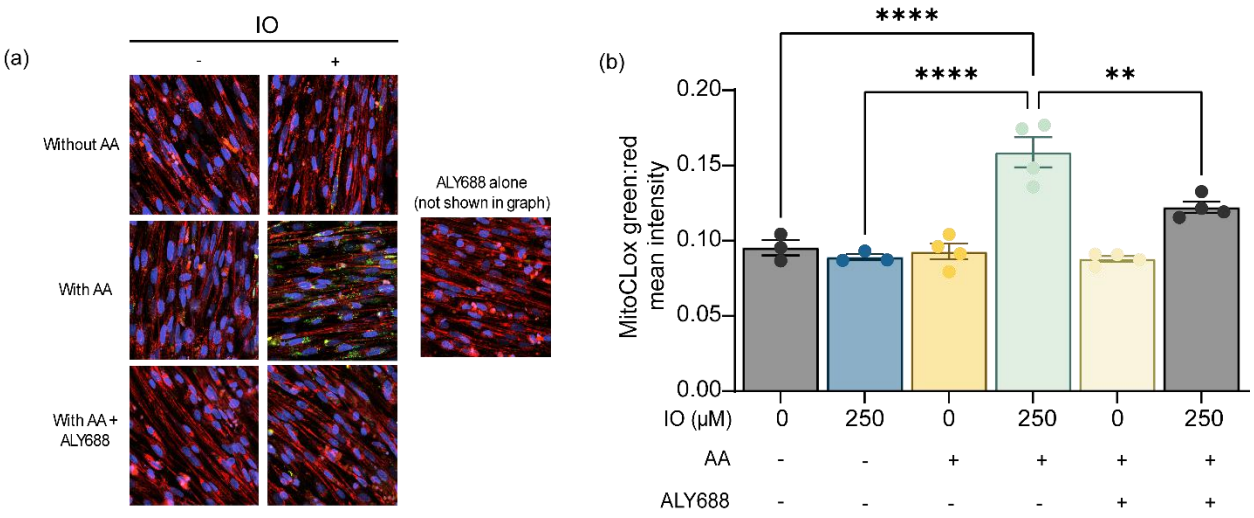

Figure 9: ALY688 attenuates mitochondria lipid peroxidation caused by AA and iron treatment in iPSC-MPs cells.

iPSC-derived myogenic progenitors (iPSC-MPs) were differentiated into myotubes within 7 days. Cells were then treated with 200 µM arachidonic acid (AA) for 24 h, followed by a 30-minute pre-treatment with 500 nM ALY688, and subsequently exposed to 0, or 250 µM $FeSO_4$ (IO) for an additional 24 h. Representative images of mitochondrial lipid peroxidation detected by mitoCLox staining ***(a)****. MitoCLox fluorescence intensity was quantified and expressed as the ratio of oxidized (green) to reduced (red) fluorescence* ***(b)****. Values are presented as mean ± SEM. **p<0.01, ****p<0.0001 (n= 3,4). (one-way ANOVA with multiple comparisons)*

The concentrations of arachidonic acid (AA) and iron ($FeSO_4$) used in iPSC-MPs were higher than those used in L6 cells. However, the combined effect of AA and iron on the induction of mitochondrial lipid peroxidation was consistent with the observations in L6 cells. This data (Figure 9 b) showed a significant increase in mitochondrial lipid peroxidation when iPSC-MPs were treated with AA and 250 µM $FeSO_4$, and this effect

was attenuated by ALY688. These findings suggest that ALY688 may exert a protective effect in human cells, similar to its effect in L6 cells.

Arachidonic acid increases susceptibility to iron induced ferroptosis in L6 cells which is prevented by ALY688

To confirm that increased lipid peroxidation and oxidative stress contribute to cell death, potentially implicating ferroptosis, cell death was measured using two complementary methods: the lactate dehydrogenase (LDH) assay and the ReadyProbes™ Cell Viability Imaging Kit. The LDH assay is based on a series of enzymatic reactions. In the first step, LDH catalyzes the oxidation of lactate to pyruvate while concurrently reducing NAD^+ to NADH. The resulting NADH then drives a second reaction, in which it reduces a tetrazolium salt to a colored formazan product in the presence of an electron-coupling reagent such as phenazine methosulfate (PMS). The reaction was quantified using a plate reader at an absorbance of 490 nm. The second method, the ReadyProbes™ Cell Viability Imaging Kit, includes two fluorescent dyes: NucBlue® Live Reagent and NucGreen® Dead Reagent. NucBlue stains the nuclei of all cells, regardless of viability, and serves as a reference for the total cell population. In contrast, NucGreen selectively stained dead cells because it can only penetrate compromised cell membranes. Cell viability was calculated by determining the percentage of NucGreen-positive cells (dead cells) relative to the total number of NucBlue-stained cells, and then multiplying by 100 to obtain the percentage of dead cells. To determine viability, this value was subtracted from 100. To validate that the observed cell death involved ferroptosis, Ferrostatin-1 (Fer-1) was included as a

positive control. Ferrrostatin-1 is a selective ferroptosis inhibitor that exerts protective effects by scavenging lipid peroxyl radicals, thereby preventing lipid peroxidation–induced cell death.

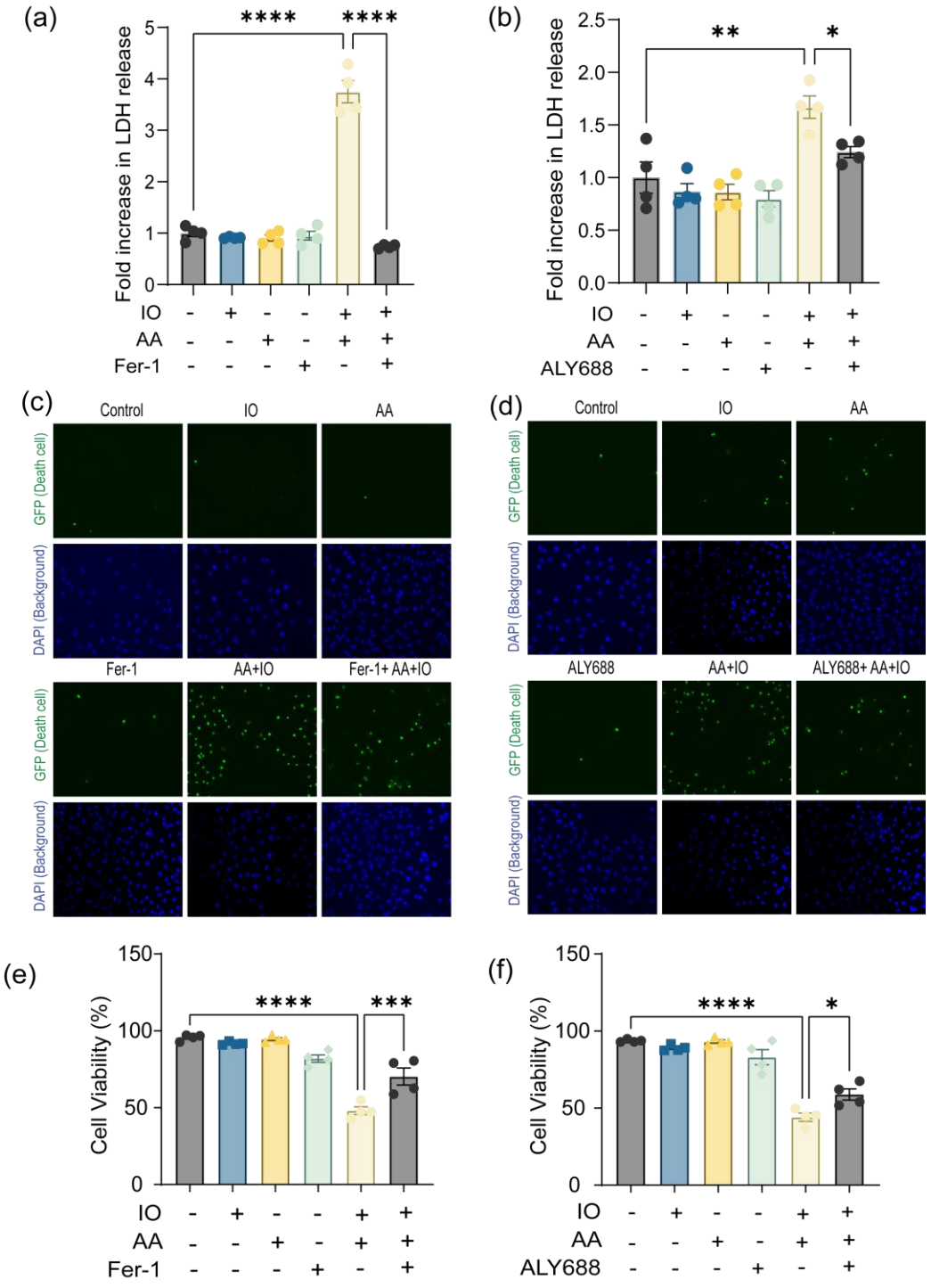

Figure 10: Arachidonic acid increases susceptibility to iron induced ferroptosis in L6 cells which is prevented by ALY688

*The fold change in LDH release was measured in L6 cells treated with 80 µM arachidonic acid (AA) for 24 h, followed by 100 µM $FeSO_4$ (IO) for an additional 24 h. Where indicated, cells were pretreated with Ferrostatin-1 (Fer-1) or ALY688 (300 nM) for 30 min prior to iron exposure. **p<0.01, ***p<0.001, ****p<0.0001 (n=4)* ***(a,b)****. Representative images of L6 cells stained with the ReadyProbes™ Cell Viability Imaging Kit under the same treatment conditions as those used in the LDH assay. NucBlue® stains the nuclei of all cells (blue), whereas NucGreen® selectively stains dead cells (green) with compromised membranes, as shown in the representative images* ***(c,d)****. Cell viability was quantified by calculating the percentage of NucGreen-positive cells (dead cells) relative to the total number of NucBlue-stained cells, and then multiplying by 100 to obtain the percentage of cell death. Viability was calculated by subtracting this value from 100%; **p<0.01, ****p<0.0001 (n=4)* ***(e,f)****. Values are presented as the mean ± SEM. (one-way ANOVA with multiple comparisons)*

The results (Figure 10 a, b) showed that treatment with either arachidonic acid (AA) or iron ($FeSO_4$) alone did not significantly increase LDH release. However, the combination of AA and iron significantly increased LDH release, indicating enhanced susceptibility to cell death. Treatment with Ferrostatin-1 (Fer-1), a known ferroptosis inhibitor used as a positive control, significantly reduced LDH release, supporting the involvement of ferroptotic cell death in this model (Figure 10 a). Notably, ALY688 significantly reduced LDH release under the same conditions (Figure 10 b). To better visualize cell death, Live/Dead staining was performed using the ReadyProbes ™ Cell Viability Imaging Kit (Figure 10 c, d). This analysis yielded results consistent with the LDH assay, showing increased cell death in the AA + iron group, which was attenuated

by both ferrostain-1(Figure 10 c,e) and ALY688 (Figure 10 d,f) treatment. Together, these results suggest that ALY688 protects against ferroptosis, similar to ferrostatin-1.

Arachidonic acid increases susceptibility to iron induced ferroptosis in iPSC-MPs which is prevented by ALY688

The results were validated using iPSC-derived myogenic progenitor cells by performing both the LDH assay and ReadyProbes™ Cell Viability staining. This was performed to validate and extend the findings observed in L6 cells and to determine whether the same effects occurred in a human cell model.

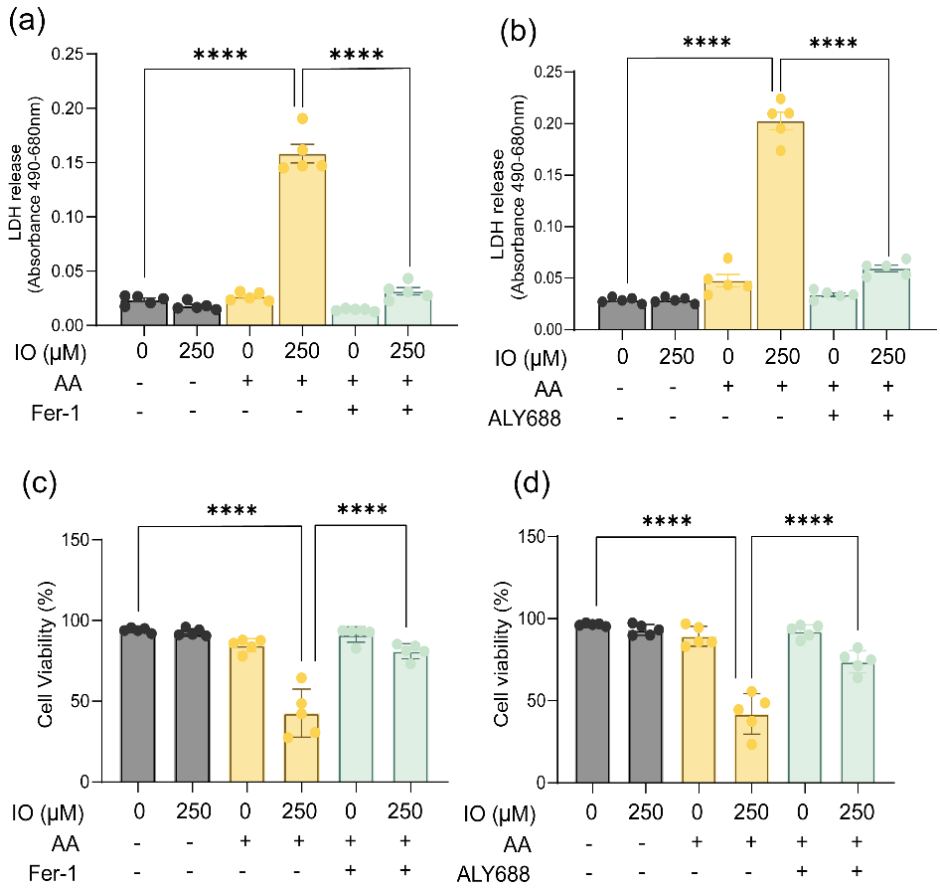

Figure 11: Arachidonic acid increases susceptibility to iron induced ferroptosis in iPSC-MPs which is prevented by ALY688

*iPSC-derived myogenic progenitors (iPSC-MPs) were differentiated into myotubes within 7 days. Cells were then treated with 200 µM arachidonic acid (AA) for 24 h, followed by a 30-minute pre-treatment with 500 nM ALY688 or Ferrosatin-1 (Fer-1) 1µM, and subsequently exposed to 0 or 250 µM $FeSO_4$ (IO) for an additional 24 h. LDH release was measured in iPSC-MPs after treatment **(a,b)**. The ReadyProbes™ Cell Viability Imaging Kit was used to evaluate cell viability. This was quantified by calculating the percentage of NucGreen-positive cells (dead cells) relative to the total number of NucBlue-stained cells, and then multiplying by 100 to obtain the percent cell death. Cell viability was calculated by subtracting this value from 100% **(c,d)**. Values are presented as the mean ± SEM. **p<0.01 (n= 5) (one-way ANOVA with multiple comparisons)*

The results showed that LDH release (Figure 11 a) was significantly increased in the AA + IO treatment group, indicating enhanced apoptosis. Pre-treatment with Ferrostatin-1 (Fer-1) effectively inhibited this increase, suggesting that cell death was ferroptosis-related, consistent with the findings in the L6 animal cell model. These results were further supported by cell viability analysis using the ReadyProbes™ Cell Viability Imaging Kit, where the AA + IO combination significantly decreased cell viability, whereas ferrostatin-1 pre-treatment significantly increased viability under the same conditions (Figure 11 c). Similarly, as shown in Figure 3.1.5b, ALY688 also demonstrated a protective effect in AA + IO–treated cells by reducing LDH release compared with the AA + IO group alone. This finding was confirmed by the ReadyProbes™ assay (Figure 11 d), which showed a significant increase in cell viability after ALY688 treatment.

Therefore, treatment with iron in combination with arachidonic acid (AA) increases lipid peroxidation and induces ferroptotic cell death in HCC cells. However, while ALY688 demonstrates a protective effect against ferroptosis, its underlying mechanism of action remains unclear and requires further investigation.

Inhibition of Nrf2 diminishes the protective effect of ALY688 against ferroptosis.

ML385 is a small molecule that specifically inhibits the transcription factor, Nrf2. It binds to the Neh1 domain of Nrf2, which belongs to the Cap 'N' Collar Basic Leucine Zipper (CNC-bZIP) family of transcription factors. This interaction disrupts the formation of the Nrf2–MAFG protein complex and impairs its ability to bind DNA regulatory elements, thereby inhibiting the transcription of Nrf2-dependent genes [125-127]. To evaluate whether the protective effect of ALY688 against ferroptosis was Nrf2-dependent, ML385 was used as a functional inhibitor. ML385 (5 μM) was administered as a 30-minute pre-treatment prior to ALY688 exposure, followed by AA and iron (IO) treatment, as described in the previous section.

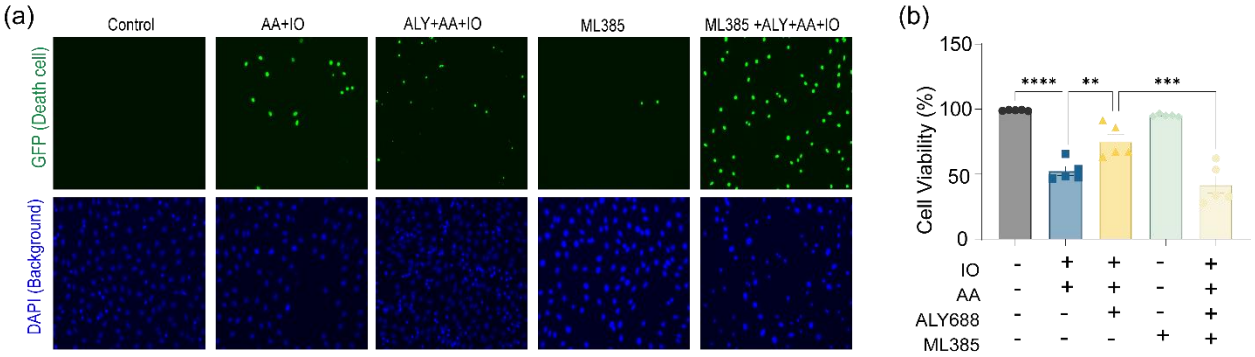

Figure 12: Inhibition of Nrf2 diminishes the protective effect of ALY688 against ferroptosis.

Representative images of L6 wild-type (L6WT) cells stained using the ReadyProbes™ Cell Viability Imaging Kit ***(a)****. L6WT cells were treated with 80 μM*

*arachidonic acid (AA) for 24 h, followed by a 30-minute pre-treatment with either 1 μM Ferrostatin-1 (Fer-1) or 300 nM ALY688. Subsequently, the cells were exposed to 5 μM ML385 (Nrf2 inhibitor) for 30 min. Finally, the cells were treated with 100 μM $FeSO_4$ (IO) for an additional 24 h **(b)**. Values are presented as the mean ± SEM. **p<0.01, ***p<0.001, ****p<0.0001 (n=5) (one-way ANOVA with multiple comparisons)*

The results showed that treatment with iron overload (IO) and arachidonic acid (AA) significantly reduced cell viability, whereas ALY688 markedly increased viability, consistent with the findings of previous experiments. ML385 treatment alone did not significantly decrease the viability of the cells. However, when ML385 was administered prior to ALY688, a significant reduction in cell viability was observed. This finding suggests that the protective effect of ALY688 against ferroptosis is likely mediated through Nrf2 activation (Figure 3.3.1 a and b).

ALY688 exerts its protective effects in both L6 cells and iPSC-derived myogenic progenitors (iPSC-MPs) through Nrf2 activation.

To generate Nrf2 reporter cells, both L6 cells and iPSC-derived myogenic progenitors (iPSC-MPs) were transfected with the plasmid pREP-8xARE-GFP-SV40-BFP, obtained from Addgene (#134910). This plasmid contains two key reporter elements: blue fluorescent protein (BFP) and green fluorescent protein (GFP). The BFP cassette is driven by the SV40 promoter, ensuring that all successfully transfected cells express blue fluorescence, which serves as a marker of the transfection efficiency. In contrast, the GFP cassette is regulated by an 8xARE (antioxidant response element)

sequence, which is activated upon Nrf2 pathway induction (Figure 13 a). Therefore, green fluorescence specifically indicates Nrf2-mediated transcriptional activity in the cells. To validate the functionality of the reporter system, CDDO-Im (CDDO imidazolide), a synthetic oleanolic acid derivative known to activate Nrf2, was used. CDDO-Im disrupts the interaction between Nrf2 and its repressor, Keap1, by modifying the reactive cysteine residues on Keap1. This allows Nrf2 to escape degradation, translocate to the nucleus, and bind ARE sequences, promoting the transcription of antioxidant genes [128, 129]. CDDO-Im was used as a positive control to confirm the responsiveness of the reporter system and compare its effect with that of ALY688.

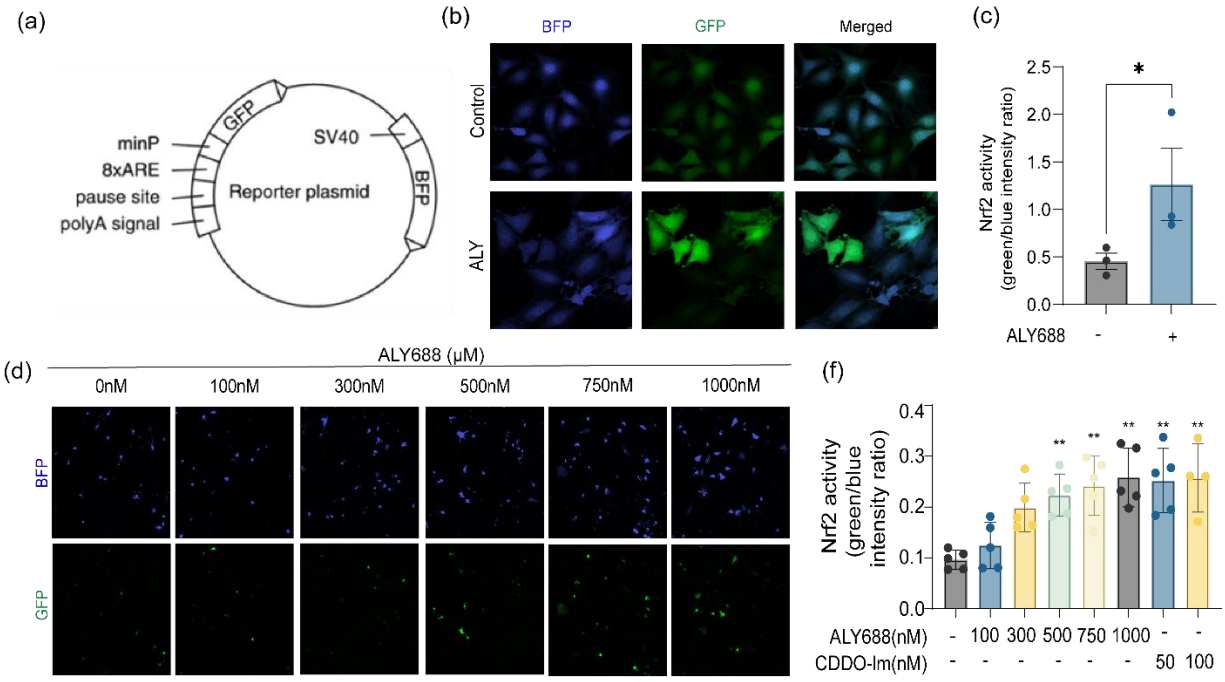

Figure 13: ALY688 exerts its protective effects in both L6 cells and iPSC-derived myogenic progenitors (iPSC-MPs) through Nrf2 activation.

Schematic representation of the pREP-8xARE-GFP-SV40-BFP plasmid used to generate Nrf2 reporter cells. Blue fluorescent protein (BFP) is driven by the SV40

promoter and serves as a marker of transfection. The GFP (green fluorescent protein) is regulated by eight copies of the antioxidant response element (ARE), allowing detection of Nrf2-mediated transcriptional activation ***(a)****. Representative image of L6 Nrf2 reporter cells treated with ALY688 (300 nM) for 24 h* ***(b)****. Nrf2 activity was assessed by the ratio of green (GFP) to blue (BFP) fluorescence intensity* ***(c)****. Values are presented as mean ± SEM. *p<0.05, n=3. Statistical differences were analyzed using paired t-test. iPSC-derived myogenic progenitors (iPSC-MPs) were transiently transfected with the same Nrf2 reporter plasmid, as shown in the representative images* ***(e)****. iPSC Nrf2 reporter cells were then treated with increasing concentrations of ALY688 (0–1000 nM) or with the Nrf2 inducer CDDO-Im (50 or 100 nM) for 4 h. Nrf2 activity was quantified as the green-to-blue fluorescence intensity ratio* ***(f)****. Values are presented as mean ± SEM. **p<0.01, n=5. (one-way ANOVA with multiple comparisons)*

The results showed that Nrf2 activity in L6 Nrf2 reporter cells was significantly increased following ALY688 treatment compared to that in the control group (Figure 13 b, c). Similarly, in iPSC-derived Nrf2 reporter cells, ALY688 treatment also led to a marked increase in Nrf2 activity, comparable to that observed in the CDDO-Im–treated groups (50 nM and 100 nM) (Figure 13 d and f). These findings confirm that ALY688 activates the Nrf2 pathway in both L6 cells and iPSC-derived myogenic progenitor cells.

ALY688 increased GSH/GSSG ratio in the AA with iron treatment.

Nrf2 target genes were associated with glutathione (GSH) synthesis and included SLC7A11, GSR, GSS, GCL, Txnrd1, and Txn1. SLC7A11 encodes a component of the sodium-independent cystine–glutamate antiporter, also known as system Xc − (xCT) [130]. This transporter facilitates the uptake of cystine in exchange for glutamate and

plays a critical role in maintaining intracellular GSH levels [131]. Glutathione reductase (GSR) reduces oxidized glutathione (GSSG) to its reduced form (GSH), preserving the cellular redox balance [132]. Glutathione synthetase (GSS) catalyzes the final step of GSH biosynthesis [133]. Glutamate-cysteine ligase (GCL), the rate-limiting enzyme in GSH biosynthesis, comprises two subunits: GCLC (catalytic subunit) provides core enzymatic activity, and GCLM (modifier subunit) enhances the catalytic efficiency (kcat) of GCLC [134]. According to previous studies, GCLC is more crucial than GCLM; germline deletion of GCLC is embryonically lethal in mice [135], and its silencing accelerates ferroptosis and promotes lung adenocarcinoma cell proliferation and invasion [136]. In contrast, GCLM knockout mice are viable and fertile under normal conditions [137], but GCLM plays a supportive role in improving GCL activity [134].

The GSH/GSSG-Glo™ Assay is a luminescence-based kit used to detect and quantify reduced glutathione (GSH) and oxidized glutathione (GSSG) levels in cells and tissues. The assay operates using a luciferin derivative (Luciferin-NT), which is converted to luciferin in the presence of GSH. This luciferin is then used in a luciferase reaction to generate a measurable luminescent signal that is proportional to the GSH concentration. To measure GSSG, a specific reagent first blocks all GSH, allowing only GSSG to be enzymatically reduced and quantified using the same luciferase-based detection method. The results were used to calculate the GSH/GSSG ratio, which serves as a key indicator of cellular redox status. A higher ratio suggests a more reduced environment, reflecting enhanced antioxidant capacity, often mediated by Nrf2 target gene activation, particularly in the GPX4-glutathione system. This was used to confirm that Nrf2-driven gene expression also translates into the functional upregulation

of downstream antioxidant systems, specifically through enhanced GSH biosynthesis and redox maintenance.

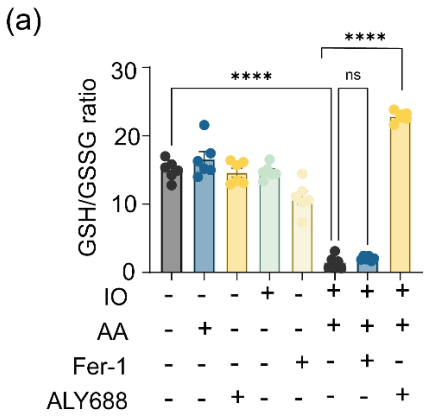

Figure 14: ALY688 increased GSH/GSSG ratio in the AA with iron treatment.

Quantification of GSH(reduced glutathione)/GSSG(oxidized glutathione) ratio of L6WT treated with 80μM arachidonic acid (AA) for 24h, followed by pre-treatment with 1μM Ferostatin-1 or ALY688 for 30 min and then 100μM FeSO4 for 24h (IO) ***(a)****. Values are mean ± SEM ****p<0.0001, n=5. (one-way ANOVA with multiple comparisons)*

The results of the GSH/GSSG-Glo™ assay (Figure 15 a) showed that individual treatment with iron (IO) or arachidonic acid (AA) did not significantly increase the GSH/GSSG ratio compared to that of the control. However, when ALY688 was administered in combination with AA and IO, there was a significant increase in intracellular GSH levels compared to the AA + IO group. These findings suggest that ALY688 activates the Nrf2 pathway, leading to the upregulation of genes involved in glutathione biosynthesis and maintaining redox homeostasis. This contributes to the restoration of intracellular GSH levels and reinforces the cell's antioxidant defense system, potentially enhancing resistance to ferroptotic stress.

2.5 Discussion

Metabolic hyperferritinemia (MHF) refers to elevated systemic iron levels (hyperferritinemia) in conjunction with metabolic syndrome (MetS) [13]. The accumulation of iron, especially when combined with metabolic dysfunctions such as dyslipidemia, may contribute to muscle mass loss and functional decline, leading to sarcopenia [22, 47, 66]. Previous studies have demonstrated that the combination of arachidonic acid (AA) and iron can synergistically promote ferroptosis. For example, in patients with cardiomyopathy and transfusion-induced iron overload, elevated AA levels are associated with increased oxidative stress [138]. Based on these findings, a model of ferroptotic cell death in skeletal muscle cells was used, in which the cells were treated with a combination of AA and iron. The concentrations of $FeSO_4$ and AA used in this study were previously validated by a former lab member, who demonstrated that this combination increases the sensitivity of lipid peroxidation in L6 cells [139, 140]. However, the underlying molecular mechanisms contributing to this increased susceptibility have not yet been fully characterized.

My results revealed that treatment with either 100 μM AA or iron alone did not significantly increase reactive oxygen species (ROS) levels. Similarly, neither treatment alone altered cellular or mitochondrial lipid peroxidation on their own. However, the combination of AA and iron led to a significant increase in ROS levels, which was associated with elevated levels of both cellular and mitochondrial lipid peroxidation. These findings suggest that mitochondria may be a central target of oxidative damage in this ferroptosis model. To further investigate the mechanisms underlying increased ferroptosis sensitivity, western blot analysis was performed on key antioxidant enzymes

involved in ferroptosis resistance, including GPX4, FSP1, and DHODH. The quantified results demonstrated that the combination of AA and iron significantly decreased GPX4 expression compared to the control, whereas the expression levels of other ferroptosis-protective mechanisms, including DHODH and FSP1, remained unchanged, even with a high dosage of iron. These findings suggest that GPX4 plays a primary role in modulating the sensitivity to ferroptosis. The lack of upregulation of backup pathway enzymes implies that DHODH and FSP1 may only become functionally dominant when GPX4 is inhibited or depleted. This is consistent with previous studies showing that DHODH and FSP1 act as compensatory ferroptosis-suppressing mechanisms in the absence of GPX4 [119, 141].

To verify the involvement of ferroptosis, ferrostatin-1, a synthetic small molecule known for scavenging lipid peroxyl radicals. Treatment with ferrostatin-1 significantly reduced both total cellular and mitochondrial lipid peroxidation in AA+ iron treatment, confirming its role as a potent ferroptosis inhibitor and suggesting that lipid peroxidation is the cause of ferroptosis in this co-treatment. Notably, this protective effect was also observed in iPSC-derived skeletal muscle cells, emphasizing the translational relevance of these findings to human cell models. Collectively, these results provide strong evidence that ferroptosis is a key mechanism of cell death under co-treatment with AA and iron.

Adiponectin is a hormone secreted by adipose tissue and is well known for its protective effects against various pathological conditions across multiple organs [75]. Its downstream signaling pathways are involved in mitigating oxidative stress and mitochondrial dysfunction, primarily through the activation of AMPK, PGC-1α, and other

antioxidant-related mechanisms [108]. In skeletal muscle, previous studies have shown that adiponectin protects against ROS and cell death through the activation of sphingosine-1-phosphate (S1P) signaling [142]. Additionally, it can prevent mitochondrial depolarization, modulate autophagy, and suppress apoptosis [143].

The development of adiponectin-based therapeutics faces several challenges, such as poor bioavailability, short half-life, and failure to meet drug safety criteria [88, 89]. To overcome these limitations, a novel adiponectin-mimetic peptide, ALY688, has been developed, showing therapeutic efficacy in various diseases, including DMD and dry eye disease [50, 86, 90]. It can activate both AdipoR1 and AdipoR2 signaling pathways, exhibiting a higher affinity than endogenous adiponectin [54, 83, 86]. The findings of this study revealed that ALY688, especially when co-treated with iron and AA, significantly reduced ROS levels. Additionally, it decreased both total and mitochondrial lipid peroxidation, indicating that its protective mechanism involves the inhibition of ferroptosis. These results align with previous studies that have highlighted the protective role of adiponectin in the skeletal muscle, particularly through its regulation of lipid peroxidation [114, 144].

The pathophysiology of various skeletal muscle diseases, such as Duchenne muscular dystrophy (DMD), cachexia, and sarcopenia, is linked to ferroptosis [35, 83]. To verify that MHF also involves ferroptosis as its pathological mechanism, LDH release and ReadyProbes™ Live/Dead assays were employed to evaluate cell viability in L6 cells and iPSC-MPs treated with AA and iron. The results demonstrated that this combination significantly enhanced ferroptotic cell death, as evidenced by increased LDH release and decreased cell viability. Notably, ferrostatin-1 effectively prevented cell

death, reinforcing the conclusion that ferroptosis is the primary mechanism responsible for cell death.

Furthermore, cell death assays, including LDH release and Live/Dead ReadyProbes™ staining, indicated that ALY688 pre-treatment markedly reduced cell death under AA and iron co-treatment conditions. Notably, this protective effect closely mirrored the effect of ferrostatin-1, suggesting that ALY688 possesses anti-ferroptotic properties in skeletal muscle. These findings align with reports from other tissues, such as the brain, liver, and breast, where adiponectin signaling has been shown to modulates ferroptosis [107, 145, 146].

The downstream signaling pathways activated by ALY688 are similar to those of native adiponectin and other adiponectin agonists, including the induction of autophagy and enhancement of insulin signaling, such as increased Akt and IRS-1 phosphorylation in response to insulin stimulation [147, 148]. This study is the first to demonstrate that ALY688 regulates ferroptosis via Nrf2 activation in skeletal muscle. Nrf2 is a well-established transcription factor that upregulates genes involved in the GPX4 antioxidant system, including SLC7A11, GCLC, and GSS, all of which are critical for glutathione biosynthesis and lipid peroxide detoxification [149].

Several studies have confirmed that Nrf2 activation modulates ferroptosis-related signaling in various pathological contexts. For example, in ischemic stroke, Nrf2 activation mitigates reperfusion injury via the Nrf2/SLC7A11/GPX4 pathway [150], whereas in myocardial ischemia-reperfusion injury, Nrf2 upregulates both SLC7A11 and GPX4, reducing ferroptosis-associated damage [151]. The connection between adiponectin and Nrf2 signaling has been well documented in various disease models. In

a cardiac hypertrophy model, adiponectin activates Nrf2, leading to cardioprotective effects in the heart. Similarly, in a mouse model of diabetic cardiomyopathy, activation of the AMPK/Nrf2 axis resulted in a reduction in ferroptosis, highlighting the role of this pathway in protecting against oxidative damage [152]. Furthermore, the resistance of hepatocarcinoma cells to radiation is associated with the upregulation of AdipoR1 following radiation exposure. This upregulation subsequently activates Nrf2 and boosts the expression of genes involved in the GPX4 antioxidant system, further highlighting the protective role of this pathway in oxidative stress [107]. Moreover, dimethyl fumarate (Tecfidera), an FDA-approved treatment for multiple sclerosis, has been found to protect against ferroptosis in hepatic and cerebral tissues through an Nrf2-dependent mechanism [153, 154]. These findings indicate that adiponectin–Nrf2 signaling is important for reducing oxidative damage and controlling genes related to ferroptosis.

The current findings highlight the skeletal muscle as another tissue in which Nrf2 signaling plays a crucial role in mitigating ferroptotic cell death. This is particularly significant, given that reduced Nrf2 activity has been associated with aging and impaired muscle function [103]. In this study, Nrf2 reporter cells were generated using L6 cells and iPSC-MP. The reporter plasmid used contained an antioxidant response element (ARE) upstream of the green fluorescent protein (GFP). When Nrf2 is activated, it binds to the ARE sequence, triggering GFP expression, which serves as a fluorescent readout of the Nrf2 activity. The results showed that ALY688 treatment significantly increased Nrf2 activity compared to the control conditions in both cell types.

ML385 is a small-molecule inhibitor of Nrf2 that blocks its ability to bind to antioxidant response elements (ARE), thereby suppressing the transcription of Nrf2

target genes [125]. In this study, treatment with ML385 in combination with ALY688 led to a significant reduction in cell viability, indicating that the cytoprotective effects of ALY688 depend on Nrf2 activation. This observation is consistent with the existing literature, where ML385 use in various cancer cell models induced reactive oxygen species (ROS) and increased sensitivity to cell death [125, 127, 155]. In contrast, CDDO-Im, a synthetic triterpenoid and potent Nrf2 activator, has been shown to upregulate Nrf2 target genes and cytoprotective proteins across multiple organs, including the liver, kidney, lung, heart, intestine, and brain, in preclinical models [128].

In this study, iPSC-derived myogenic progenitor (iPSC-MP) reporter cells treated with ALY688 showed GFP expression comparable to that of CDDO-Im, confirming that ALY688 is a potent inducer of Nrf2 activity in human skeletal muscle cells.

Furthermore, Nrf2 activation by ALY688 restored intracellular GSH levels which associated with the GPX4 antioxidant system, reinforcing its role in resistance to ferroptosis. Taken together, these findings suggest that ALY688 promotes Nrf2 signaling to protect cells against oxidative stress and ferroptosis. Thus, pharmacological strategies aimed at enhancing Nrf2 activity, such as ALY688, may hold strong therapeutic potential for preventing or delaying age-associated muscle degeneration, including sarcopenia.

In conclusion, this study explored the potential of the adiponectin receptor agonist ALY688 to protect skeletal muscle cells from ferroptosis and the underlying mechanisms involved. Using iPSC-derived and L6 skeletal muscle cells, we demonstrated that AA increased susceptibility to IO-induced oxidative stress, lipid peroxidation, and ferroptosis. The use of ALY688 conferred protection against the

induction of these changes following treatment with AA and IO. Furthermore, ALY688 might activates the Nrf2 signaling pathway to upregulate antioxidant genes that confer anti-ferroptotic properties. Inhibition of Nrf2 activity abolished ALY688's protective effects. Therefore, ALY688 protects against AA- and IO-induced ferroptosis in skeletal muscle cells via Nrf2 signaling.

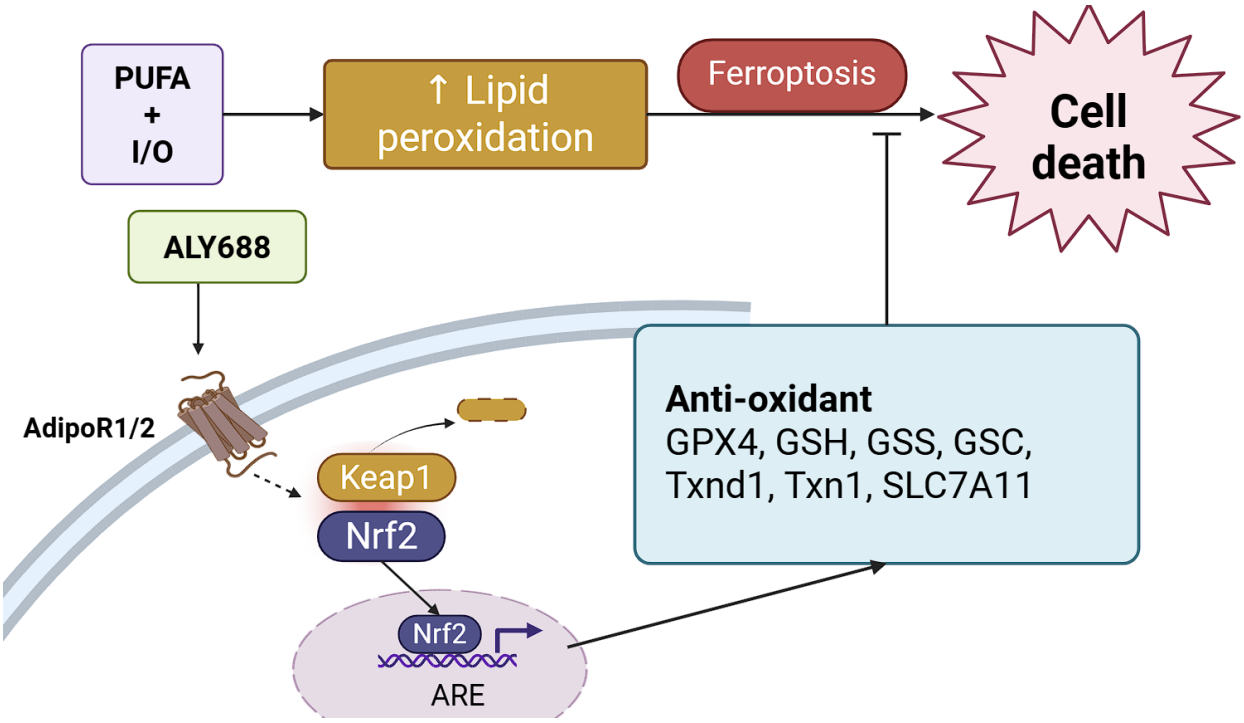

Figure 15: Summarized the mechanism involved in this study.

Schematic illustration of ALY688-mediated protection against ferroptosis via Nrf2 signaling pathway activation. Polyunsaturated fatty acids (PUFAs) and iron overload (I/O) enhance lipid peroxidation, which drives ferroptosis and subsequent cell death. ALY688 activates AdipoR1/2 receptors, leading to disruption of the Keap1–Nrf2 complex and allowing Nrf2 nuclear translocation. In the nucleus, Nrf2 binds to antioxidant response elements (AREs) and induces the transcription of antioxidant genes, including GPX4, GSH, GSS, GSC, Txnrd1, Txn1, and SLC7A11. These antioxidant proteins mitigate lipid peroxidation and suppress ferroptosis, thereby promoting cell survival.

Chapter 3: Final Remarks and Future Plans

This study investigated ferroptotic cell death induced by a combination of iron and arachidonic acid and the protective role of the adiponectin receptor agonist ALY688, mediated through Nrf2 activation. This experimental model is designed to mimic metabolic hyperferritinemia (MHF), a condition that often originates from metabolic disorders and progresses to iron overload (IO). By replicating the key features of MHF at the cellular level, this study contributes to a deeper understanding of the molecular mechanisms underlying ferroptosis in skeletal muscle and highlights the potential of Nrf2-targeted therapies, such as ALY688, for ameliorating oxidative stress and preventing cell death in iron-associated metabolic diseases.

In this study, we investigated the role of lipid peroxidation induced by polyunsaturated fatty acids (PUFAs) in altering ferroptosis susceptibility. However, there remains a significant opportunity for further exploration. It is well established that phosphatidylethanolamine (PE) lipid peroxides are key effectors of oxidative stress and major contributors to ferroptosis [42, 43]. To gain deeper insights into lipid-driven ferroptotic mechanisms, lipidomic analyses should be employed in future studies. This approach would allow for the identification of specific lipid molecular species altered during AA and iron co-treatment and further determine how these profiles are modified by ALY688. In addition, proteomic analysis could be valuable as a broad screening tool to detect upregulated or downregulated proteins in response to ferroptotic stress and ALY688 intervention. This could reveal previously unrecognized signaling pathways or regulatory networks involved in iron-induced lipid peroxidation, offering new mechanistic insights and identifying potential therapeutic targets. Together, these omics approaches

will expand our understanding of the molecular landscape of ferroptosis and the mechanisms by which ALY688 modulates oxidative stress responses at both lipid and protein levels.

Nrf2 activity has been shown to increase following ALY688 treatment. To further explore the relationship between Nrf2 and ferroptosis, additional experiments could incorporate CDDO-Im, a well-established Nrf2 activator, to evaluate its effects on protective enzymes, such as GPX4. Previous studies have demonstrated that Nrf2 silencing significantly reduces GPX4 expression in the mouse liver, supporting the role of Nrf2 in regulating the key components of the ferroptosis defense system [156]. In this study, ALY688 treatment significantly increased the GSH/GSSG ratio, indicating an enhanced cellular antioxidant capacity, likely driven by increased glutathione synthesis. However, to validate this effect, a direct comparison with CDDO-Im is warranted to determine Nrf2-mediated antioxidant gene expression. This gene expression analyses should reveal that ALY688 upregulated key genes in the GSH/GPX4 axis, a well-established pathway for protection against ferroptosis.

The Nrf2-activating properties of ALY688 observed in this study should be further validated in vivo studies. Previous research in mice has shown that Nrf2 activation protects against high-fat diet–induced obesity, emphasizing its role in metabolic regulation and oxidative stress defense [157, 158]. Additionally, Nrf2 knockout mice exhibit a 30% reduction in muscle performance and a 68% increase in reactive oxygen species (ROS) compared to wild-type controls, demonstrating the critical role of Nrf2 in skeletal muscle function [159]. However, in vivo studies exploring the interaction between Nrf2 and adiponectin signaling in skeletal muscle, particularly in the context of

ferroptosis, are lacking. Future studies should investigate the pharmacodynamics of ALY688, focusing on drug diffusion, tissue-specific targeting, and optimal dosage in skeletal muscles. One experimental approach would be to administer ALY688 to mice and compare Nrf2-regulated protein expression in skeletal muscle tissue between the treated and control groups. In addition, muscle strength and function can be assessed using aging or metabolic syndrome mouse models, which are expected to exhibit features of metabolic hyperferritinemia (MHF). Measuring ferritin levels in these animals would help confirm the presence of MHF, allowing for a comparison of muscle performance between the ALY688-treated and untreated groups. Such a study would offer valuable insights into the pharmacological effects of ALY688 in a more complex physiological system, thereby improving our understanding of its potential therapeutic value in age-related muscle degeneration and iron-related metabolic disorders.

This study also holds translational potential for clinical research, offering a foundation for understanding ferroptosis and MHF in humans. Indeed, I will be responsible for a new project which is currently ongoing in Thailand in collaboration with Dr. Sweeney's lab. As part of the clinical investigation, patients with sarcopenia (and age-matched controls) are being enrolled and assessed for a range of blood biomarkers, including the metabolic syndrome panel (fasting blood glucose, HbA1c, HDL, triglycerides, and LDL), ferritin levels, and adiponectin levels. In addition, plasma samples collected from these patients are being analyzed to identify novel biological markers that may be associated with iron regulation and muscle regeneration. Previous studies have reported changes in PF4 and C1R levels in exosomes of patients with sarcopenia, although these markers are more strongly linked to the inflammatory

response [160]. The goal of this study will be to identify potential biomarkers that have a strong correlation between MHF and sarcopenia, which may provide additional insight into the pathogenesis of sarcopenia.

In summary, the study presented in this thesis provides valuable insights into the mechanisms of ferroptotic cell death induced by iron and arachidonic acid and the protective role of ALY688 through Nrf2 activation. The experimental model mimicking metabolic hyperferritinemia (MHF) has enhanced our understanding of ferroptosis in skeletal muscle and highlighted the potential of Nrf2-targeted therapy for iron-associated metabolic diseases. But the further the further investigation into the pathophysiology of this diseases have to be done more in vitro and in vivo. This comprehensive approach, which combines basic science with clinical investigations, may lead to new therapeutic strategies for age-related muscle degeneration and iron-related metabolic disorders, ultimately improving patient outcomes.

References

1. Huang, P.L., *A comprehensive definition for metabolic syndrome.* Dis Model Mech, 2009. **2**(5-6): p. 231-7.

2. Wilson, R.H., R.W. Stream, and D.D. Dirks, *Spread-of-masking effects on pure tones and several speech stimuli.* J Speech Hear Res, 1973. **16**(3): p. 385-96.

3. Grundy, S.M., et al., *Diagnosis and management of the metabolic syndrome: an American Heart Association/National Heart, Lung, and Blood Institute Scientific Statement.* Circulation, 2005. **112**(17): p. 2735-52.

4. Zhu, L., et al., *The IDF Definition Is Better Suited for Screening Metabolic Syndrome and Estimating Risks of Diabetes in Asian American Adults: Evidence from NHANES 2011-2016.* J Clin Med, 2020. **9**(12).

5. Grundy, S.M., et al., *Definition of metabolic syndrome: Report of the National Heart, Lung, and Blood Institute/American Heart Association conference on scientific issues related to definition.* Circulation, 2004. **109**(3): p. 433-8.

6. Rao, D.P., et al., *Metabolic syndrome and chronic disease.* Chronic Dis Inj Can, 2014. **34**(1): p. 36-45.

7. Riediger, N.D. and I. Clara, *Prevalence of metabolic syndrome in the Canadian adult population.* CMAJ : Canadian Medical Association journal = journal de l'Association medicale canadienne, 2011. **183**(15).

8. Zhou, B., S. Liu, and G. Yuan, *Combined Associations of Serum Ferritin and Body Size Phenotypes With Cardiovascular Risk Profiles: A Chinese Population-Based Study.* Front Public Health, 2021. **9**: p. 550011.

9. Wrede, C.E., et al., *Association between serum ferritin and the insulin resistance syndrome in a representative population.* Eur J Endocrinol, 2006. **154**(2): p. 333-40.

10. Jehn, M., J.M. Clark, and E. Guallar, *Serum ferritin and risk of the metabolic syndrome in U.S. adults.* Diabetes Care, 2004. **27**(10): p. 2422-8.

11. Haap, M., et al., *Insulin sensitivity and liver fat: role of iron load.* J Clin Endocrinol Metab, 2011. **96**(6): p. E958-61.

12. Sachinidis, A., et al., *Dysmetabolic Iron Overload in Metabolic Syndrome.* Curr Pharm Des, 2020. **26**(10): p. 1019-1024.

13. Valenti, L., et al., *Consensus Statement on the definition and classification of metabolic hyperferritinaemia.* Nat Rev Endocrinol, 2023. **19**(5): p. 299-310.

14. Mendler, M.H., et al., *Insulin resistance-associated hepatic iron overload.* Gastroenterology, 1999. **117**(5): p. 1155-63.

15. Jezequel, C., et al., *Both hepatic and body iron stores are increased in dysmetabolic iron overload syndrome. A case-control study.* PLoS One, 2015. **10**(6): p. e0128530.

16. Deugnier, Y., É. Bardou-Jacquet, and F. Lainé, *Dysmetabolic iron overload syndrome (DIOS).* La Presse Médicale, 2017. **46**(12): p. e306-e311.

17. Anastasopoulos, N.A., et al., *Exploring the Role of Metabolic Hyperferritinaemia (MHF) in Steatotic Liver Disease (SLD) and Hepatocellular Carcinoma (HCC).* Cancers (Basel), 2025. **17**(5).

18. Turlin, B., et al., *Histologic features of the liver in insulin resistance-associated iron overload. A study of 139 patients.* Am J Clin Pathol, 2001. **116**(2): p. 263-70.

19. Deugnier, Y. and B. Turlin, *Pathology of hepatic iron overload.* World J Gastroenterol, 2007. **13**(35): p. 4755-60.

20. Sangkhae, V. and E. Nemeth, *Regulation of the Iron Homeostatic Hormone Hepcidin.* Adv Nutr, 2017. **8**(1): p. 126-136.

21. Deugnier, Y., E. Bardou-Jacquet, and F. Laine, *Dysmetabolic iron overload syndrome (DIOS).* Presse Med, 2017. **46**(12 Pt 2): p. e306-e311.

22. Ikeda, Y., et al., *Iron-induced skeletal muscle atrophy involves an Akt-forkhead box O3-E3 ubiquitin ligase-dependent pathway.* Journal of trace elements in medicine and biology : organ of the Society for Minerals and Trace Elements (GMS), 2016. **35**: p. 66-76.

23. Sung, H.K., et al., *Autophagy deficiency exacerbates iron overload induced reactive oxygen species production and apoptotic cell death in skeletal muscle cells.* Cell Death & Disease 2023 14:4, 2023. **14**(4): p. 1-13.

24. Li, J., et al., *Ferroptosis: past, present and future.* Cell Death & Disease 2020 11:2, 2020. **11**(2): p. 1-13.

25. Dixon, S.J., et al., *Ferroptosis: an iron-dependent form of nonapoptotic cell death.* Cell, 2012. **149**(5): p. 1060-1072.

26. Overmeyer, J.H. and W.A. Maltese, *Death Pathways Triggered by Activated Ras in Cancer Cells.* Frontiers in bioscience : a journal and virtual library, 2011. **16**(5): p. 1693-1693.

27. Puig, S., et al., *The elemental role of iron in DNA synthesis and repair.* Metallomics, 2017. **9**(11): p. 1483-1500.

28. Zhao, G., *Is Iron Accumulation a Possible Risk Factor for Sarcopenia?* Biological Trace Element Research, 2018. **186**(2): p. 379-383.

29. Kalpage, H.A., et al., *Cytochrome c phosphorylation: Control of mitochondrial electron transport chain flux and apoptosis.* Int J Biochem Cell Biol, 2020. **121**: p. 105704.

30. Nemeth, E. and T. Ganz, *Hepcidin-Ferroportin Interaction Controls Systemic Iron Homeostasis.* Int J Mol Sci, 2021. **22**(12).

31. Camaschella, C., A. Nai, and L. Silvestri, *Iron metabolism and iron disorders revisited in the hepcidin era.* Haematologica, 2020. **105**(2): p. 260-272.

32. Ganz, T., *Systemic iron homeostasis.* Physiol Rev, 2013. **93**(4): p. 1721-41.

33. Gingoyon, A., et al., *Chronic Iron Deficiency and Cognitive Function in Early Childhood.* Pediatrics, 2022. **150**(6).

34. Auerbach, M., T.G. DeLoughery, and J.S. Tirnauer, *Iron Deficiency in Adults: A Review.* JAMA, 2025. **333**(20): p. 1813-1823.

35. Wang, Y., et al., *Ferroptosis and its role in skeletal muscle diseases.* Frontiers in Molecular Biosciences, 2022. **9**: p. 1051866-1051866.

36. Galy, B., M. Conrad, and M. Muckenthaler, *Mechanisms controlling cellular and systemic iron homeostasis.* Nature Reviews Molecular Cell Biology 2023 25:2, 2023. **25**(2): p. 133-155.

37. Trostchansky, A., I. Wood, and H. Rubbo, *Regulation of arachidonic acid oxidation and metabolism by lipid electrophiles.* Prostaglandins & Other Lipid Mediators, 2021. **152**: p. 106482-106482.

38. Kagan, V.E., et al., *Oxidized arachidonic and adrenic PEs navigate cells to ferroptosis.* Nature chemical biology, 2017. **13**(1): p. 81-90.

39. Seibt, T.M., B. Proneth, and M. Conrad, *Role of GPX4 in ferroptosis and its pharmacological implication.* Free radical biology & medicine, 2019. **133**: p. 144-152.

40. Black, P.N. and C.C. DiRusso, *Transmembrane Movement of Exogenous Long-Chain Fatty Acids: Proteins, Enzymes, and Vectorial Esterification.* Microbiology and Molecular Biology Reviews, 2003. **67**(3): p. 454-472.

41. Costa, I., et al., *Molecular mechanisms of ferroptosis and their involvement in brain diseases.* Pharmacology & Therapeutics, 2023. **244**: p. 108373-108373.

42. Yang, W.S. and B.R. Stockwell, *Ferroptosis: Death by Lipid Peroxidation.* Trends in cell biology, 2016. **26**(3): p. 165-176.

43. Bruni, A., et al., *Ferroptosis-inducing agents compromise in vitro human islet viability and function.* Cell death & disease, 2018. **9**(6).

44. Yang, W.S. and B.R. Stockwell, *Synthetic Lethal Screening Identifies Compounds Activating Iron-Dependent, Nonapoptotic Cell Death in Oncogenic-RAS-Harboring Cancer Cells.* Chemistry & Biology, 2008. **15**(3): p. 234-245.

45. Jiang, L., et al., *Dynamic roles of p53-mediated metabolic activities in ROS-induced stress responses.* Cell Cycle, 2015. **14**(18): p. 2881-2881.

46. Liu, M.r., W.t. Zhu, and D.s. Pei, *System Xc−: a key regulatory target of ferroptosis in cancer.* Investigational New Drugs, 2021. **39**(4): p. 1123-1131.

47. DeRuisseau, K.C., et al., *Aging-related changes in the iron status of skeletal muscle.* Experimental Gerontology, 2013. **48**(11): p. 1294-1302.

48. Scherer, P.E., et al., *A novel serum protein similar to C1q, produced exclusively in adipocytes.* The Journal of biological chemistry, 1995. **270**(45): p. 26746-26749.

49. Liu, Y., V. Vu, and G. Sweeney, *Examining the Potential of Developing and Implementing Use of Adiponectin-Targeted Therapeutics for Metabolic and Cardiovascular Diseases.* Frontiers in Endocrinology, 2019. **10**: p. 481842-481842.

50. Dubuisson, N., et al., *The Adiponectin Receptor Agonist, ALY688: A Promising Therapeutic for Fibrosis in the Dystrophic Muscle.* Cells, 2023. **12**(16): p. 2101-2101.

51. Fang, X., et al., *Hyperglycemia- and hyperinsulinemia-induced alteration of adiponectin receptor expression and adiponectin effects in L6 myoblasts.* Journal of molecular endocrinology, 2005. **35**(3): p. 465-476.

52. Straub, L.G. and P.E. Scherer, *Metabolic Messengers: Adiponectin.* Nature metabolism, 2019. **1**(3): p. 334-339.

53. McEntegart, M.B., et al., *Increase in serum adiponectin concentration in patients with heart failure and cachexia: relationship with leptin, other cytokines, and B-type natriuretic peptide.* European heart journal, 2007. **28**(7): p. 829-835.

54. Otvos, L., et al., *Design and development of a peptide-based adiponectin receptor agonist for cancer treatment.* BMC biotechnology, 2011. **11**(1): p. 90-90.

55. Dong, H., et al., *Nrf2 inhibits ferroptosis and protects against acute lung injury due to intestinal ischemia reperfusion via regulating SLC7A11 and HO-1.* Aging, 2020. **12**(13): p. 12943-12959.

56. Feng, L., et al., *SLC7A11 regulated by NRF2 modulates esophageal squamous cell carcinoma radiosensitivity by inhibiting ferroptosis.* Journal of Translational Medicine, 2021. **19**(1): p. 1-16.

57. Frontera, W.R. and J. Ochala, *Skeletal muscle: a brief review of structure and function.* Calcif Tissue Int, 2015. **96**(3): p. 183-95.

58. Halon-Golabek, M., et al., *Iron Metabolism of the Skeletal Muscle and Neurodegeneration.* Front Neurosci, 2019. **13**: p. 165.

59. Ryan, B.J., et al., *Skeletal muscle ferritin abundance is tightly related to plasma ferritin concentration in adults with obesity.* Exp Physiol, 2020. **105**(11): p. 1808-1814.

60. Walston, J.D., *Sarcopenia in older adults.* Curr Opin Rheumatol, 2012. **24**(6): p. 623-7.

61. Chen, L.-K., et al., *Asian Working Group for Sarcopenia: 2019 Consensus Update on Sarcopenia Diagnosis and Treatment.* Journal of the American Medical Directors Association, 2020. **21**(3): p. 300-307.e2.

62. Cruz-Jentoft, A.J., et al., *Sarcopenia: revised European consensus on definition and diagnosis.* Age Ageing, 2019. **48**(1): p. 16-31.

63. Beaudart, C., et al., *Health Outcomes of Sarcopenia: A Systematic Review and Meta-Analysis.* PLoS One, 2017. **12**(1): p. e0169548.

64. Huang, Y., et al., *Ferroptosis in a sarcopenia model of senescence accelerated mouse prone 8 (SAMP8).* Int J Biol Sci, 2021. **17**(1): p. 151-162.

65. Ding, H., et al., *Transferrin receptor 1 ablation in satellite cells impedes skeletal muscle regeneration through activation of ferroptosis.* J Cachexia Sarcopenia Muscle, 2021. **12**(3): p. 746-768.

66. Alves, F.M., et al., *Age-Related Changes in Skeletal Muscle Iron Homeostasis.* J Gerontol A Biol Sci Med Sci, 2023. **78**(1): p. 16-24.

67. Wang, Y., et al., *Ferroptosis and its role in skeletal muscle diseases.* Front Mol Biosci, 2022. **9**: p. 1051866.

68. Lambertucci, R.H., et al., *Effects of moderate electrical stimulation on reactive species production by primary rat skeletal muscle cells: cross talk between superoxide and nitric oxide production.* Journal of cellular physiology, 2012. **227**(6): p. 2511-2518.

69. Won, C.W., *Management of Sarcopenia in Primary Care Settings.* Korean J Fam Med, 2023. **44**(2): p. 71-75.

70. Khoramipour, K., et al., *Adiponectin: Structure, Physiological Functions, Role in Diseases, and Effects of Nutrition.* Nutrients, 2021. **13**(4).

71. Liu, M. and F. Liu, *Regulation of adiponectin multimerization, signaling and function.* Best Pract Res Clin Endocrinol Metab, 2014. **28**(1): p. 25-31.

72. Yamauchi, T., et al., *Cloning of adiponectin receptors that mediate antidiabetic metabolic effects.* Nature, 2003. **423**(6941): p. 762-769.

73. Keshvari, S., et al., *Muscle-specific overexpression of AdipoR1 or AdipoR2 gives rise to common and discrete local effects whilst AdipoR2 promotes additional systemic effects.* Sci Rep, 2017. **7**: p. 41792.

74. Ruan, H. and L.Q. Dong, *Adiponectin signaling and function in insulin target tissues.* J Mol Cell Biol, 2016. **8**(2): p. 101-9.

75. Kadowaki, T. and T. Yamauchi, *Adiponectin and adiponectin receptors.* Endocr Rev, 2005. **26**(3): p. 439-51.

76. Chial, H.J., et al., *Membrane targeting by APPL1 and APPL2: dynamic scaffolds that oligomerize and bind phosphoinositides.* Traffic, 2008. **9**(2): p. 215-29.

77. Diggins, N.L. and D.J. Webb, *APPL1 is a multifunctional endosomal signaling adaptor protein.* Biochem Soc Trans, 2017. **45**(3): p. 771-779.

78. Zhou, L., et al., *Adiponectin activates AMP-activated protein kinase in muscle cells via APPL1/LKB1-dependent and phospholipase C/Ca2+/Ca2+/calmodulin-dependent protein kinase kinase-dependent pathways.* J Biol Chem, 2009. **284**(33): p. 22426-22435.

79. Patel, S.A., et al., *Overexpression of the adiponectin receptor AdipoR1 in rat skeletal muscle amplifies local insulin sensitivity.* Endocrinology, 2012. **153**(11): p. 5231-46.

80. Civitarese, A.E., et al., *Role of adiponectin in human skeletal muscle bioenergetics.* Cell Metab, 2006. **4**(1): p. 75-87.

81. Abou-Samra, M., et al., *Potential Therapeutic Action of Adiponectin in Duchenne Muscular Dystrophy.* Am J Pathol, 2017. **187**(7): p. 1577-1585.

82. Gamberi, T., F. Magherini, and T. Fiaschi, *Adiponectin in Myopathies.* Int J Mol Sci, 2019. **20**(7).

83. Bellissimo, C.A., et al., *The slow-release adiponectin analog ALY688-SR modifies early-stage disease development in the D2.mdx mouse model of Duchenne muscular dystrophy.* Am J Physiol Cell Physiol, 2024. **326**(4): p. C1011-C1026.

84. Komici, K., et al., *Adiponectin and Sarcopenia: A Systematic Review With Meta-Analysis.* Front Endocrinol (Lausanne), 2021. **12**: p. 576619.

85. Tanaka, Y., et al., *Author Correction: Adiponectin promotes muscle regeneration through binding to T-cadherin.* Sci Rep, 2020. **10**(1): p. 12219.

86. Kumar, P., et al., *Adiponectin agonist ADP355 attenuates CCl4-induced liver fibrosis in mice.* PloS one, 2014. **9**(10).

87. Bellissimo, C.A., et al., *The adiponectin analogue ALY688-SR attenuates diaphragm fibrosis, atrophy and mitochondrial stress in a mouse model of Duchenne muscular dystrophy.* bioRxiv, 2023: p. 2023.05.22.541826-2023.05.22.541826.

88. Salmons, H.I., et al., *The Safety of Adiponectin Receptor Agonist AdipoRon in a Rabbit Model of Arthrofibrosis.* Tissue Eng Part C Methods, 2023. **29**(4): p. 154-159.

89. Huang, Z., et al., *The adiponectin-derived peptide ALY688 protects against the development of metabolic dysfunction-associated steatohepatitis.* Clin Transl Sci, 2024. **17**(6): p. e13760.

90. Sall, K., et al., *A Phase 1/2a Study of ALY688 Ophthalmic Solution in Dry Eye Subjects.* Investigative Ophthalmology & Visual Science, 2023. **64**(8): p. 3959-3959.

91. Yan, R., et al., *NRF2, a Superstar of Ferroptosis.* Antioxidants, 2023. **12**(9): p. 1739-1739.

92. Katsuoka, F., et al., *Genetic Evidence that Small Maf Proteins Are Essential for the Activation of Antioxidant Response Element-Dependent Genes.* Molecular and Cellular Biology, 2005. **25**(18): p. 8044-8051.

93. Nam, L.B. and Y.S. Keum, *Binding partners of NRF2: Functions and regulatory mechanisms.* Archives of Biochemistry and Biophysics, 2019. **678**: p. 108184-108184.

94. Salazar, M., et al., *Glycogen Synthase Kinase-3β Inhibits the Xenobiotic and Antioxidant Cell Response by Direct Phosphorylation and Nuclear Exclusion of the Transcription Factor Nrf2.* Journal of Biological Chemistry, 2006. **281**(21): p. 14841-14851.

95. McMahon, M., et al., *Keap1-dependent Proteasomal Degradation of Transcription Factor Nrf2 Contributes to the Negative Regulation of Antioxidant Response Element-driven Gene Expression.* Journal of Biological Chemistry, 2003. **278**(24): p. 21592-21600.

96. Moore, S., et al., *The CHD6 chromatin remodeler is an oxidative DNA damage response factor.* Nature Communications 2019 10:1, 2019. **10**(1): p. 1-16.

97. Kobayashi, M., et al., *Identification of the interactive interface and phylogenic conservation of the Nrf2-Keap1 system.* Genes to Cells, 2002. **7**(8): p. 807-820.

98. Zhang, D.D. and M. Hannink, *Distinct Cysteine Residues in Keap1 Are Required for Keap1-Dependent Ubiquitination of Nrf2 and for Stabilization of Nrf2 by Chemopreventive Agents and Oxidative Stress.* Molecular and Cellular Biology, 2003. **23**(22): p. 8137-8151.

99. Dinkova-Kostova, A.T., et al., *Direct evidence that sulfhydryl groups of Keap1 are the sensors regulating induction of phase 2 enzymes that protect against carcinogens and oxidants.* Proceedings of the National Academy of Sciences of the United States of America, 2002. **99**(18): p. 11908-11913.

100. Komatsu, M., et al., *The selective autophagy substrate p62 activates the stress responsive transcription factor Nrf2 through inactivation of Keap1.* Nature Cell Biology 2010 12:3, 2010. **12**(3): p. 213-223.

101. Ngo, V. and M.L. Duennwald, *Nrf2 and Oxidative Stress: A General Overview of Mechanisms and Implications in Human Disease.* Antioxidants, 2022. **11**(12): p. 2345-2345.

102. Itoh, K., et al., *An Nrf2/small Maf heterodimer mediates the induction of phase II detoxifying enzyme genes through antioxidant response elements.* Biochemical and Biophysical Research Communications, 1997. **236**(2): p. 313-322.

103. Huang, D.D., et al., *Nrf2 deficiency exacerbates frailty and sarcopenia by impairing skeletal muscle mitochondrial biogenesis and dynamics in an age-dependent manner.* Exp Gerontol, 2019. **119**: p. 61-73.

104. Huang, D.D., et al., *Nrf2 deficiency promotes the increasing trend of autophagy during aging in skeletal muscle: a potential mechanism for the development of sarcopenia.* Aging (Albany NY), 2020. **12**(7): p. 5977-5991.

105. Yamada, M., et al., *Muscle-derived IL-1beta regulates EcSOD expression via the NBR1-p62-Nrf2 pathway in muscle during cancer cachexia.* J Physiol, 2024. **602**(17): p. 4215-4235.

106. Pun, N.T. and P.H. Park, *Role of p62 in the suppression of inflammatory cytokine production by adiponectin in macrophages: Involvement of autophagy and p21/Nrf2 axis.* Scientific reports, 2017. **7**(1).

107. Feng, H., et al., *AdipoR1 Regulates Ionizing Radiation-Induced Ferroptosis in HCC cells through Nrf2/xCT Pathway.* Oxidative medicine and cellular longevity, 2022. **2022**.

108. Ouedraogo, R., et al., *Adiponectin suppression of high-glucose-induced reactive oxygen species in vascular endothelial cells: evidence for involvement of a cAMP signaling pathway.* Diabetes, 2006. **55**(6): p. 1840-6.

109. Hildebrandt, M.R., et al., *Precision Health Resource of Control iPSC Lines for Versatile Multilineage Differentiation.* Stem Cell Reports, 2019. **13**(6): p. 1126-1141.

110. Palacin-Martinez, C., et al., *Frontiers | The characterization of CellROX™ probes could be a crucial factor in ram sperm quality assessment.* Frontiers in Veterinary Science, 2024/02/27. **11**.

111. Dezest, M., et al., *Mechanistic insights into the impact of Cold Atmospheric Pressure Plasma on human epithelial cell lines.* Sci Rep, 2017. **7**: p. 41163.

112. Skouta, R., et al., *Ferrostatins inhibit oxidative lipid damage and cell death in diverse disease models.* J Am Chem Soc, 2014. **136**(12): p. 4551-6.

113. Anderson, E.J., L.A. Katunga, and M.S. Willis, *Mitochondria as a source and target of lipid peroxidation products in healthy and diseased heart.* Clin Exp Pharmacol Physiol, 2012. **39**(2): p. 179-93.

114. Huan, H., et al., *Mitochondrial lipid peroxidation is necessary but not sufficient for induction of ferroptosis.* Front Cell Dev Biol, 2024. **12**: p. 1452824.

115. Lyamzaev, K.G., et al., *MitoCLox: A Novel Mitochondria-Targeted Fluorescent Probe for Tracing Lipid Peroxidation.* Oxid Med Cell Longev, 2019. **2019**: p. 9710208.

116. Ma, T., et al., *GPX4-independent ferroptosis-a new strategy in disease's therapy.* Cell Death Discov, 2022. **8**(1): p. 434.

117. Xie, Y., et al., *GPX4 in cell death, autophagy, and disease.* Autophagy, 2023. **19**(10): p. 2621-2638.

118. Wang, C., et al., *DHODH Alleviates Heart Failure via the Modulation of CoQ-Related Ferroptotic Inhibition.* Front Biosci (Landmark Ed), 2024. **29**(7): p. 267.

119. Mao, C., et al., *DHODH-mediated ferroptosis defence is a targetable vulnerability in cancer.* Nature, 2021. **593**(7860): p. 586-590.

120. Littarru, G.P. and L. Tiano, *Bioenergetic and antioxidant properties of coenzyme Q10: recent developments.* Mol Biotechnol, 2007. **37**(1): p. 31-7.

121. Doll, S., et al., *FSP1 is a glutathione-independent ferroptosis suppressor.* Nature, 2019. **575**(7784): p. 693-698.

122. Li, W., et al., *FSP1: a key regulator of ferroptosis.* Trends Mol Med, 2023. **29**(9): p. 753-764.

123. Zeng, F., X. Chen, and G. Deng, *The anti-ferroptotic role of FSP1: current molecular mechanism and therapeutic approach.* Mol Biomed, 2022. **3**(1): p. 37.

124. Cerneckis, J., H. Cai, and Y. Shi, *Induced pluripotent stem cells (iPSCs): molecular mechanisms of induction and applications.* Signal Transduct Target Ther, 2024. **9**(1): p. 112.

125. Taufani, I.P., et al., *Mitochondrial ROS induced by ML385, an Nrf2 inhibitor aggravates the ferroptosis induced by RSL3 in human lung epithelial BEAS-2B cells.* Hum Exp Toxicol, 2023. **42**: p. 9603271221149663.

126. Singh, A., et al., *Small Molecule Inhibitor of NRF2 Selectively Intervenes Therapeutic Resistance in KEAP1-Deficient NSCLC Tumors.* ACS Chem Biol, 2016. **11**(11): p. 3214-3225.

127. Xu, C., et al., *ML385, an Nrf2 Inhibitor, Synergically Enhanced Celastrol Triggered Endoplasmic Reticulum Stress in Lung Cancer Cells.* ACS Omega, 2024. **9**(43): p. 43697-43705.

128. Thimmulappa, R.K., et al., *Preclinical evaluation of targeting the Nrf2 pathway by triterpenoids (CDDO-Im and CDDO-Me) for protection from LPS-induced inflammatory response and reactive oxygen species in human peripheral blood mononuclear cells and neutrophils.* Antioxid Redox Signal, 2007. **9**(11): p. 1963-70.

129. Xu, D., et al., *The triterpenoid CDDO-imidazolide ameliorates mouse liver ischemia-reperfusion injury through activating the Nrf2/HO-1 pathway enhanced autophagy.* Cell Death Dis, 2017. **8**(8): p. e2983.

130. Thimmulappa, R.K., et al., *Nrf2-dependent protection from LPS induced inflammatory response and mortality by CDDO-Imidazolide.* Biochem Biophys Res Commun, 2006. **351**(4): p. 883-9.

131. Lewerenz, J., P. Maher, and A. Methner, *Regulation of xCT expression and system x (c) (-) function in neuronal cells.* Amino Acids, 2012. **42**(1): p. 171-9.

132. Han, C., et al., *GSR is not essential for the maintenance of antioxidant defenses in mouse cochlea: Possible role of the thioredoxin system as a functional backup for GSR.* PLoS One, 2017. **12**(7): p. e0180817.

133. De Jesus, M.C., et al., *The role of strong electrostatic interactions at the dimer interface of human glutathione synthetase.* Protein J, 2014. **33**(5): p. 403-9.

134. Lee, J.I., J. Kang, and M.H. Stipanuk, *Differential regulation of glutamate-cysteine ligase subunit expression and increased holoenzyme formation in response to cysteine deprivation.* Biochem J, 2006. **393**(Pt 1): p. 181-90.

135. Chen, Y., et al., *Oral N-acetylcysteine rescues lethality of hepatocyte-specific Gclc-knockout mice, providing a model for hepatic cirrhosis.* J Hepatol, 2010. **53**(6): p. 1085-94.

136. Luo, L., et al., *Ferroptosis-Related Gene GCLC Is a Novel Prognostic Molecular and Correlates with Immune Infiltrates in Lung Adenocarcinoma.* Cells, 2022. **11**(21).

137. Yang, Y., et al., *Initial characterization of the glutamate-cysteine ligase modifier subunit Gclm(-/-) knockout mouse. Novel model system for a severely compromised oxidative stress response.* J Biol Chem, 2002. **277**(51): p. 49446-52.

138. Mattera, R., et al., *Increased release of arachidonic acid and eicosanoids in iron-overloaded cardiomyocytes.* Circulation, 2001. **103**(19): p. 2395-401.

139. De Menezes Reboucas, P. and G. Sweeney, *Examining the Impact of PUFAs and the Role of Autophagy in Iron-Induced Ferroptotic Cell Death*. 2022: Toronto.

140. Yan, Y., G. Lei, and B. Gan, *A mTORC1-mediated cyst(e)ine sensing mechanism governing GPX4 synthesis and ferroptosis.* Mol Cell Oncol, 2021. **8**(3): p. 1919006.

141. Tian, R.L., et al., *Temsirolimus inhibits FSP1 enzyme activity to induce ferroptosis and restrain liver cancer progression.* J Mol Cell Biol, 2025. **16**(8).

142. Botta, A., et al., *An adiponectin-S1P autocrine axis protects skeletal muscle cells from palmitate-induced cell death.* Lipids Health Dis, 2020. **19**(1): p. 156.

143. Ren, Y., et al., *Adiponectin modulates oxidative stress-induced mitophagy and protects C2C12 myoblasts against apoptosis.* Sci Rep, 2017. **7**(1): p. 3209.

144. Liu, Y. and G. Sweeney, *Adiponectin action in skeletal muscle.* Best Pract Res Clin Endocrinol Metab, 2014. **28**(1): p. 33-41.

145. Ge, Y., et al., *Adiponectin ameliorates traumatic brain injury-induced ferroptosis through AMPK- ACC1 signaling pathway.* Brain Behav Immun, 2025. **126**: p. 160-175.

146. Chung, S.J., et al., *ADIPOQ/adiponectin induces cytotoxic autophagy in breast cancer cells through STK11/LKB1-mediated activation of the AMPK-ULK1 axis.* Autophagy, 2017. **13**(8): p. 1386-1403.

147. Tam, E., M. Ouimet, and G. Sweeney, *Cardioprotective Effects of Adiponectin-Stimulated Autophagy.* J Lipid Atheroscler, 2025. **14**(1): p. 40-53.

148. Sung, H.K., et al., *ALY688 elicits adiponectin-mimetic signaling and improves insulin action in skeletal muscle cells.* Am J Physiol Cell Physiol, 2022. **322**(2): p. C151-C163.

149. Loboda, A., et al., *Role of Nrf2/HO-1 system in development, oxidative stress response and diseases: an evolutionarily conserved mechanism.* Cell Mol Life Sci, 2016. **73**(17): p. 3221-47.

150. Liu, H., et al., *Rhein attenuates cerebral ischemia-reperfusion injury via inhibition of ferroptosis through NRF2/SLC7A11/GPX4 pathway.* Exp Neurol, 2023. **369**: p. 114541.

151. Yao, D., et al., *Isoliquiritigenin alleviates myocardial ischemia-reperfusion injury by regulating the Nrf2/HO-1/SLC7a11/GPX4 axis in mice.* Free Radic Biol Med, 2024. **221**: p. 1-12.

152. Li, H., et al., *Adiponectin ameliorates hyperglycemia-induced cardiac hypertrophy and dysfunction by concomitantly activating Nrf2 and Brg1.* Free Radic Biol Med, 2015. **84**: p. 311-321.

153. Qi, D., et al., *Dimethyl fumarate protects against hepatic ischemia-reperfusion injury by alleviating ferroptosis via the NRF2/SLC7A11/HO-1 axis.* Cell Cycle, 2023. **22**(7): p. 818-828.

154. Yan, N., et al., *Dimethyl fumarate improves cognitive deficits in chronic cerebral hypoperfusion rats by alleviating inflammation, oxidative stress, and ferroptosis via NRF2/ARE/NF-kappaB signal pathway.* Int Immunopharmacol, 2021. **98**: p. 107844.

155. Yan, L., et al., *ML385 promotes ferroptosis and radiotherapy sensitivity by inhibiting the NRF2-SLC7A11 pathway in esophageal squamous cell carcinoma.* Med Oncol, 2024. **41**(12): p. 309.

156. Zhao, T., et al., *Regulating Nrf2-GPx4 axis by bicyclol can prevent ferroptosis in carbon tetrachloride-induced acute liver injury in mice.* Cell Death Discov, 2022. **8**(1): p. 380.

157. Yu, Z., et al., *Oltipraz upregulates the nuclear factor (erythroid-derived 2)-like 2 [corrected](NRF2) antioxidant system and prevents insulin resistance and obesity induced by a high-fat diet in C57BL/6J mice.* Diabetologia, 2011. **54**(4): p. 922-34.

158. Shin, S., et al., *Role of Nrf2 in prevention of high-fat diet-induced obesity by synthetic triterpenoid CDDO-imidazolide.* Eur J Pharmacol, 2009. **620**(1-3): p. 138-44.

159. Crilly, M.J., et al., *The role of Nrf2 in skeletal muscle contractile and mitochondrial function.* J Appl Physiol (1985), 2016. **121**(3): p. 730-40.

160. Aparicio, P., et al., *Proteomic profiling of human plasma extracellular vesicles identifies PF4 and C1R as novel biomarker in sarcopenia.* J Cachexia Sarcopenia Muscle, 2024. **15**(5): p. 1883-1897.

Appendix A: Statement of Contributions

I would like to acknowledge Eddie Tam, our laboratory technician, for his invaluable contributions to this study. He collaborated on the culture, treatment, and confocal microscopy imaging of iPSC-derived cells (Figure 3.1.5, Figure 3.1.7). He also assisted with capturing confocal microscopy images of L6 cells (Figure 3.1.1 a, 3.1.2 a, 3.1.3 a, and 3.2.2 b).

Appendix B: Permission for use of adapted or reproduced figures from websites or articles

Figure 2: Adapted from Valenti, L., et al (2023) [13]. Open Access article.

Valenti, L., et al., *Consensus Statement on the definition and classification of metabolic hyperferritinaemia*. Nat Rev Endocrinol, 2023. **19**(5): p. 299-310.

‣ Nat Rev Endocrinol. 2023 Feb 17;19(5):299–310. doi: 10.1038/s41574-023-00807-6

Consensus Statement on the definition and classification of metabolic hyperferritinaemia

Luca Valenti [1,2,3,✉], Elena Corradini [4,5,✉], Leon A Adams [6], Elmar Aigner [7], Saleh Alqahtani [8,9], Marco Arrese [10], Edouard Bardou-Jacquet [11], Elisabetta Bugianesi [12], Jose-Manuel Fernandez-Real [13,14,15,16], Domenico Girelli [17], Hannes Hagström [18], Benjamin Henninger [19], Kris Kowdley [20,21], Guido Ligabue [4,22], Donald McClain [23,24], Fabrice Lainé [25], Koji Miyanishi [26], Martina U Muckenthaler [27,28,29], Alessia Pagani [30], Patrizia Pedrotti [31], Antonello Pietrangelo [4,5], Daniele Prati [3], John D Ryan [32], Laura Silvestri [30], C Wendy Spearman [33], Per Stål [18], Emmanuel A Tsochatzis [34], Francesca Vinchi [35,36], Ming-Hua Zheng [37,38], Heinz Zoller [39,40]

‣ Author information ‣ Article notes ‣ Copyright and License information

PMCID: PMC9936492 PMID: 36805052

SPRINGER NATURE LICENSE
TERMS AND CONDITIONS

Aug 02, 2025

This Agreement between Photsathorn Haetanurak ("You") and Springer Nature ("Springer Nature") consists of your license details and the terms and conditions provided by Springer Nature and Copyright Clearance Center.

License Number	6080900444561
License date	Aug 02, 2025
Licensed Content Publisher	Springer Nature
Licensed Content Publication	Nature Reviews Endocrinology
Licensed Content Title	Consensus Statement on the definition and classification of metabolic hyperferritinaemia
Licensed Content Author	Luca Valenti et al
Licensed Content Date	Feb 17, 2023
Type of Use	Thesis/Dissertation
Requestor type	academic/university or research institute
Format	electronic
Portion	figures/tables/illustrations
Number of figures/tables/illustrations	1
Would you like a high resolution image with your order?	no
Will you be translating?	no
Circulation/distribution	1 - 29
Author of this Springer Nature content	no
Title of new work	The adiponectin receptor agonist ALY688 protects against iron-induced ferroptosis via Nrf2 activation in skeletal muscle
Institution name	York University
Expected presentation date	Aug 2025
Portions	Figure 1
The Requesting Person / Organization to Appear on the License	Photsathorn Haetanurak
Requestor Location	Mr. Photsathorn Haetanurak 100/883 Moo 5, Soi 53A Bang Kruai - Sai Noi Rd Bang Rak Phatthana Bang Bua Thong, Nonthaburi 11110 Thailand
Customer Tax ID	TH1101700220648
Billing Type	Invoice
Billing Address	Mr. Photsathorn Haetanurak 100/883 Moo 5, Soi 53A Bang Kruai - Sai Noi Rd Bang Rak Phatthana Bang Bua Thong, Thailand 11110
Total	**0.00 USD**

Terms and Conditions

Springer Nature Customer Service Centre GmbH Terms and Conditions

The following terms and conditions ("Terms and Conditions") together with the terms specified in your [RightsLink] constitute the License ("License") between you as Licensee and Springer Nature Customer Service Centre GmbH as Licensor. By clicking 'accept' and completing the transaction for your use of the material ("Licensed Material"), you confirm your acceptance of and obligation to be bound by these Terms and Conditions.

1. Grant and Scope of License

Figure 3: Retrieved and adapted from Lugano, G. (2025) BioRender. Open Access template.

Lugano, G. (2025). Ferroptosis Signaling Pathway. https://app.biorender.com/biorender-templates/details/t-63d6f5981de2f51833c45793-ferroptosis-signaling-pathway

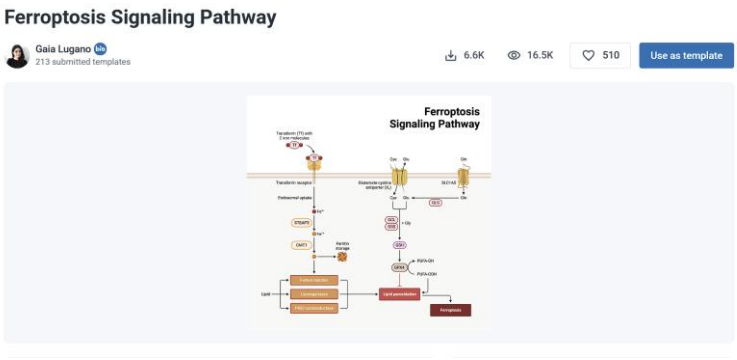

Figure 4: Retrieved from Ona, S. (2025) BioRender. Open Access template.

Ona, S. (2025). Keap1–Nrf2 Pathway. https://app.biorender.com/biorender-templates/details/t-5fbd5fbebe6dbc00a4d9cced-keap1-nrf2-pathway